

1 **Clearance of defective muscle stem cells by senolytics reduces the**
2 **expression of senescence-associated secretory phenotype and restores**
3 **myogenesis in myotonic dystrophy type 1.**

4

5 Talita C. Conte^{1,2}, Gilberto Duran-Bishop^{1,3}, Zakaria Orfi^{1,2}, Inès Mokhtari^{1,4,5}, Alyson
6 Deprez^{1,2}, Marie-Pier Roussel^{5,6}, Isabelle Côté⁵, Ornella Pellerito¹, Damien Maggiorani^{1,2},
7 Basma Benabdallah¹, Severine Leclerc¹, Lara Feulner¹, Jean Mathieu^{5,7}, Cynthia
8 Gagnon^{5,7}, Gregor Andelfinger^{1,8}, Christian Beauséjour^{1,2}, Serge McGraw^{1,3}, Elise
9 Duchesne^{4,5,10}, and Nicolas A. Dumont^{1,9,10}

10

- 11 1. CHU Sainte-Justine Research Center. Montreal, QC, Canada.
12 2. Department of pharmacology and physiology, Faculty of Medicine, Université
13 de Montréal. Montreal, QC, Canada.
14 3. Department of obstetrics and gynecology. Faculty of Medicine, Université de
15 Montréal. Montreal, QC, Canada.
16 4. Department of Health Sciences, Université du Québec à Chicoutimi, QC,
17 Canada
18 5. Neuromuscular diseases interdisciplinary research group (GRIMN), Saguenay
19 Lac-St-Jean integrated university health and social services hospital, QC,
20 Canada.
21 6. Department of Fondamental Sciences, Université du Québec à Chicoutimi, QC,
22 Canada

23 7. CHU Sherbrooke Research Center, Faculty of Medicine and Health Sciences,

24 Université de Sherbrooke, Québec, Canada

25 8. Department of Pediatrics, Faculty of Medicine, Université de Montréal.

26 Montreal, QC, Canada.

27 9. School of rehabilitation, Faculty of Medicine, Université de Montréal.

28 Montreal, QC, Canada

29 10. These authors contributed equally

30

31 Correspondence should be addressed to N.A.D.: nicolas.dumont.1@umontreal.ca and/or

32 E.D: elise1_duchesne@uqac.ca

33

34

35 **ABSTRACT**

36 Muscle weakness and atrophy are clinical hallmarks of myotonic dystrophy type 1 (DM1).
37 Muscle stem cells, which contribute to skeletal muscle growth and repair, are also affected
38 in this disease. However, the molecular mechanisms leading to this defective activity and
39 the impact on the disease severity are still elusive. Here, we explored through an unbiased
40 approach the molecular signature leading to myogenic cell defects in DM1. Single cell
41 RNAseq data revealed the presence of a specific subset of DM1 myogenic cells expressing
42 a senescence signature, characterized by the high expression of genes related to
43 senescence-associated secretory phenotype (SASP). This profile was confirmed using
44 different senescence markers *in vitro* and *in situ*. Accumulation of intranuclear RNA foci
45 in senescent cells, suggest that RNA-mediated toxicity contribute to senescence induction.
46 High expression of IL-6, a prominent SASP cytokine, in the serum of DM1 patients was
47 identified as a biomarker correlating with muscle weakness and functional capacity
48 limitations. Drug screening revealed that the BCL-XL inhibitor (A1155463), a senolytic
49 drug, can specifically target senescent DM1 myoblasts to induce their apoptosis and reduce
50 their SASP. Removal of senescent cells re-established the myogenic function of the non-
51 senescent DM1 myoblasts, which displayed improved proliferation and differentiation
52 capacity *in vitro*; and enhanced engraftment following transplantation *in vivo*. Altogether
53 this study presents a well-defined senescent molecular signature in DM1 untangling part
54 of the pathological mechanisms observed in the disease; additionally, we demonstrate the
55 therapeutic potential of targeting these defective cells with senolytics to restore
56 myogenesis.

58 **INTRODUCTION**

59 Myotonic dystrophy type 1 (DM1) is a rare disease that affects approximately 1:8,000
60 individuals in the world^{1,2}. DM1 is caused by an unstable (CTG) nucleotide repeat in the
61 *dystrophia myotonica protein kinase (DMPK)* gene³. CTG repeats in DNA lead to toxic
62 mRNA accumulation causing splicing defects mainly attributable to binding protein
63 sequestration. In healthy individuals, the *DMPK* alleles have 5 to 37 CTG repeats, but in
64 DM1, there can be hundreds to thousands of these repeats; with the number of repeats
65 partially correlating with the age of onset and the severity of the disease⁴⁻⁷. Patients are
66 classified into five clinical phenotypes according to the CTG expansion size, and the
67 occurrence and onset of their main symptoms: congenital, infantile, juvenile, adult and late-
68 onset⁸.

69

70 DM1 is a multisystemic disease that affects different organs, and particularly the skeletal
71 muscles, leading to progressive weakness and atrophy⁹. Muscle stem cells (MuSC), which
72 contribute to skeletal muscle growth and repair are also affected in this disease⁵. In healthy
73 condition, quiescent MuSC are activated after an injury and become myoblasts that
74 proliferate extensively before exiting cell cycle to self-renew or to differentiate and fuse to
75 form new myofibers¹⁰. Previous studies performed on mixed cell populations (non-purified
76 by FACS) extracted from skeletal muscle samples of DM1 patients showed that these cells
77 exhibit signs of cellular senescence (a state of irreversible cell cycle arrest), such as
78 enzymatic senescence-associated β-Galactosidase (SA-β-Gal) activity, expression of the
79 cell cycle inhibitor p16, loss of nuclear integrity, and nuclear envelope invagination^{11,12}. It
80 was shown using *in vitro* models of DM1 that cellular senescence is independent from

81 telomere shortening but is rather induced by the activity of the cell cycle inhibitor p16
82 and/or p21 in response to CTG-related stress¹²⁻¹⁴. This increase in cellular senescence is
83 associated with reduced proliferative capacity of DM1 myoblasts and delayed
84 differentiation and fusion into myofibers^{5,12,14}. Overexpression of cyclin-dependent kinase
85 4 (Cdk4) to bypass p16-induced senescence restored the proliferation of DM1 cells to the
86 level of healthy control cells¹².

87

88 In addition to decreasing the pool of competent cells, senescent cells secrete a broad range
89 of molecules including proinflammatory cytokines (e.g., IL-1, IL-6) and matrix proteinases
90 (e.g., MMP1, MMP3). This cocktail, known as the Senescence-Associated Secretory
91 Phenotype (SASP), alters the microenvironment and leads to detrimental changes in
92 neighbouring cells and in the whole organism^{15,16}. Particularly, IL-6 is associated with
93 muscle wasting conditions and promote the exhaustion of the MuSC pool¹⁷⁻¹⁹. Chronic
94 exposure to SASP is considered as one of the major sources of deleterious effects on tissue
95 maintenance and regenerative capacity^{15,20}; however, its impact on DM1 pathogenesis has
96 not been investigated yet.

97

98 Considering that senescent cells accumulate with time and have detrimental impacts on
99 neighbouring cells, they represent an attractive target for the treatment of many disorders²¹.
100 Pioneer studies showed that genetic removal of senescent cells expressing the cell cycle
101 inhibitor p16 in aging mice enhances their lifespan^{20,22}. Moreover, pharmacological
102 compounds, called senolytics, can selectively eliminate senescent cells²³, which reduces
103 the production of frailty-related proinflammatory cytokines in aged mice, and improves

104 physical function and lifespan²⁴. Considering that DM1 has been described as a progeroid
105 syndrome (i.e. mimicking premature aging)²⁵, and that skeletal muscles in DM1 share
106 many similarities with aged muscles such as cellular senescence, MuSC defects, and
107 muscle wasting²⁶, it suggests that senolytics hold great therapeutic potential for the
108 treatment of DM1. However, the impact of senolytics in muscular diseases such as DM1
109 has never been investigated.

110

111 Here, we generated the first single-cell transcriptomic atlas of DM1 to identify the
112 molecular signature of myogenic cell subpopulations. Using myoblasts isolated from DM1
113 patients and age- and sex-matched healthy controls, we identified a specific subset of
114 senescent-like cells expressing high levels of SASP. We confirmed cellular senescence
115 using different markers (p16, p21, SA- β -Gal) in primary myoblasts of DM1 patients *in*
116 *vitro* and in skeletal muscle biopsies *in situ*. Furthermore, we demonstrated that the level
117 of IL-6, a key SASP cytokine, is correlated with upper- and lower-limb muscle weakness
118 as well as functional capacity limitations in patients affected by DM1. Thereafter, we
119 screened different senolytic drugs and have identified the B-cell lymphoma-extra large
120 (BCL-XL) inhibitor, A1155463, as the most promising molecule to eliminate specifically
121 senescent myoblasts cultured from DM1 patients' samples, without affecting cells cultured
122 from healthy controls' samples. Elimination of senescent cells reduced SASP expression
123 and restored the myogenesis potential of the myoblasts *in vitro* and following cell
124 transplantation *in vivo*. Altogether, these findings support the importance of cellular
125 senescence in the disease severity, and the therapeutic potential of senolytics to target
126 defective myogenic cells and reduce SASP expression in DM1.

127 **RESULTS**

128 **Single-Cell RNAseq identifies a subset of senescent cells in DM1 myoblasts.**

129 Considering that cellular senescence only affects a subset of cells at a given moment, we
130 took advantage of the single-cell RNA sequencing (scRNAseq) technology to identify the
131 distinct transcriptional profile in cellular subpopulations of DM1 myoblasts. Myoblasts
132 were sorted by FACS (Suppl. Fig. 1) and purity was confirmed by immunofluorescence
133 (Suppl. Fig. 2). Single-cell transcriptomic sequencing was performed on pooled myoblasts
134 at the same early passage (P4) from 3 DM1 patients (juvenile phenotype) and 3 age- and
135 sex-matched healthy controls (Suppl. Table 1). After filtering and removal of doublets in
136 the sequencing data, we analysed 1,613 control cells and 1,714 DM1 patient cells (Suppl.
137 Fig. 3). Both controls and DM1 cells express high levels of myogenic cell markers such as
138 *CD82*, *ITGB1* (*CD29*), *MYF5*, *MYOD1*, *NCAM1* (*CD56*), and *DES*, as well as low levels
139 of the fibroadipogenic (*PDGFRa* and *CD34*), endothelial (*CD31* and *TIE1*), and myeloid
140 (*CD11B* and *CD45*) cell markers (Suppl. Fig. 4). UMAP plot of merged control and patient
141 cells revealed that these cells cluster differently (Fig. 1A). Differential expression analysis
142 revealed that the expression of 516 genes was significantly changed ($P < 10e-6$; $n=266$
143 downregulated and $n=250$ upregulated) in DM1 patients compared to controls (Fig. 1B,
144 Suppl. Table 2). Compared to healthy control cells, DM1 cells showed lower expression in
145 genes associated to myogenic markers (e.g., *MYF5*, *MYOD1*, *MYF6*, *SIX1*), extracellular
146 matrix components (e.g., *COL1A1*, *COL1A2*, *COL3A1*, *COL5A2*, *LAMA2*, *FNI*), Notch
147 signalling (e.g., *HEYL*, *RBPJ*), and cell cycle (e.g., *CENPF*, *CCNA2*, *CCNB1*, *CCNB2*,
148 *CDK1*, *MKI67*) (Fig 1B,C; suppl. table 2). Downregulated genes in DM1 cells were
149 enriched for biological processes related to cell cycle, muscle structure development, and

150 extracellular matrix organization (Fig 1D,F). Top upregulated genes in DM1 cells included
151 cytokines/chemokines related to inflammation (e.g., *CXCL1*, *CXCL2*, *CXCL3*, *CXCL5*,
152 *CXCL6*, *CXCL8*, *IL1B*, *IL6*, *CSF3*), and metalloproteinases (e.g., *MMP1*, *MMP3*) (Fig 1
153 B,C; suppl. table 2). Upregulated genes in DM1 cells were enriched for biological functions
154 included cytokine signaling, cellular response to stress, autophagy, apoptosis, and
155 senescence (Fig 1E,G). SCENIC analysis was used to predict transcription factors
156 regulating the gene sets. Results showed that downregulated genes are controlled by
157 different transcriptions factors related to myogenesis (e.g., MYF5, MYOD1, MYF6,
158 SIX1), while for the genes upregulated in DM1 the transcriptions factors related to the NF-
159 kB pathway (e.g., NFKB1, NFKB2, REL, RELB) were identified (Fig. 1H,I).

160 UMAP plot showed that cells expressing high levels of pro-inflammatory cytokines
161 (e.g., *CXCL1*, *CXCL8*, *IL6*) in DM1 patients are restricted to specific cell clusters (Fig.
162 1C). Further, *SAA1* and *SAA2*, two target genes of pro-inflammatory molecules such as IL-
163 1, IL-6, and TNF α ²⁷, are also upregulated in specific subsets of DM1 myogenic cells. To
164 further explore this senescent-like phenotype we compared the different clusters to gene
165 sets related to cellular senescence and SASP production²⁸. Based on this profile, we were
166 able to classify the DM1 cells in 3 subpopulations: one subset of fully senescent cells
167 expressing high levels of senescent genes and SASP (clusters 2, 3, 6), one subset of early-
168 senescent cells expressing senescence markers that did not transcribe into SASP cytokine
169 secretion (cluster 4), and one subset non-senescent cells (clusters 0, 1, 5) (Fig. 2 A-D). By
170 comparing the molecular signature of the senescent and non-senescent clusters versus all
171 the combined clusters found in our control sample, we observed a clear senescent
172 molecular signature present only in the senescent cluster (*CXCL1*, *CXCL3*, *CXCL5*,

173 *CXCL8, MMP1, SOD2*); and that the non-senescent cluster in DM1 samples expressed a
174 similar molecular profile as our control sample (Fig. 2E).

175 Production of SASP by senescent cells varies depending on the cell type and
176 inducer^{29,30}. Thus, we selected all the top differentially expressed genes (>1.7-fold) in DM1
177 and controls samples and we investigated the presence of these genes in the SASP Atlas³⁰,
178 a proteomic database that analysed the SASP factors secreted by different cell types
179 (fibroblasts and epithelial cells) subjected to multiple senescence inducers (irradiation,
180 oncogene-induced, treatment-induced). These findings indicate that the top genes
181 overexpressed in DM1 patients (e.g., *STC1, SOD2, MMP1, CXCL5, CXCL8*) are canonical
182 SASP markers expressed at the protein level by senescent cells, regardless of the cell type
183 or the senescence inducer (Suppl. Fig. 5A). On the other hand, the top upregulated genes
184 in healthy control myoblasts (e.g., *COL3A1, TOP2A*) are negative regulators of cellular
185 senescence in the SASP Atlas (Suppl. Fig. 5B).

186

187 **Cellular senescence is associated with reduced myogenesis in DM1.**

188 As single-cell analysis revealed distinct molecular signatures associated to cellular
189 senescence in DM1 cells, we further explore how this process was affected in myogenic
190 cells *in vitro* and *in situ*. First, we performed SA- β -Gal assay on myoblasts *in vitro*, and
191 we observed an 11-fold increase ($p = 0.0023$) in the proportion of β -Gal + senescent cells
192 in patient-derived DM1 myoblasts compared to healthy controls (Fig. 3A-B). Further
193 expression analysis on cultured myoblasts confirmed that *P16* is significantly upregulated
194 ($p = 0.046$) in DM1 compared to controls (Fig. 3C). As senescence is characterized by cell
195 cycle arrest, myoblast proliferation was assessed using a live cell imaging system

196 (IncuCyte), and the results showed a significant reduction ($p = 0.042$) in cell proliferation
197 in DM1 patients compared to controls (Fig. 3D).

198 To determine if the accumulation of toxic RNA is the cause of cellular senescence
199 in DM1, the number of intranuclear RNA foci was compared in senescent (SA- β -Gal+)
200 and non-senescent (SA- β -Gal-) DM1 myoblasts. A 4-fold increase ($p = 0.0017$) was
201 observed in the number of RNA foci/cell in senescent DM1 cells compared to non-
202 senescent cells (Fig. 3E,F, and suppl. Fig. 6).

203 Thereafter, cellular senescence markers were assessed on flash frozen skeletal
204 muscle biopsies to determine if senescence is also a feature of the disease *in situ*.
205 Immunofluorescence staining on skeletal muscle section showed a 5-fold increase
206 ($p=0.022$) in the proportion of satellite cells (PAX7+) co-expressing the cell cycle inhibitor
207 P16 (Fig. 3G,H) in DM1 muscles compared to controls. Gene expression analysis of
208 skeletal muscle biopsies confirmed a significant upregulation in the expression of the cell
209 cycle inhibitors *P16* (5-fold; $p=0.0075$) and *P21* (17-fold; $p=0.004$) in samples from DM1
210 patients compared to controls (Fig. 3I).

211

212 **SASP production is correlated with muscle weakness in DM1 patients.**

213 To determine the impact of SASP production on muscle function *in vivo*, blood
214 serum from DM1 patients ($n=103$; suppl. table 3) was collected to measure the level of
215 expression of IL-6, a prominent SASP cytokine. Thereafter, the maximum isometric
216 muscle strength of different muscle groups of the lower limb (ankle dorsiflexors, hip
217 flexors, knee extensors, knee flexors) and upper limb (shoulder flexors, shoulder abductors,
218 elbow flexors, elbow extensors) was quantitatively assessed. Using equations that adjust

219 for age, sex, and weight, the predicted strength value of each muscle group was calculated,
220 which allowed to identify a relative deficit compared to normative value³¹. For the lower
221 limb, a significant negative correlation between IL-6 levels and predicted maximal muscle
222 strength was observed for ankle dorsiflexors ($R: -0.426$; $p<0.001$), hip flexors ($R: -0.397$;
223 $p<0.001$), knee extensors ($R: -0.273$; $p=0.006$), and knee flexors ($R: -0.300$; $p=0.002$) (Fig.
224 4A-D). For the upper limb, a significant negative correlation was observed for shoulder
225 flexors ($R: -0.405$; $p<0.001$), shoulder abductors ($R: -0.370$; $p<0.001$), elbow flexors ($R: -$
226 0.337 ; $p<0.001$), and elbow extensors ($R: -0.407$; $p<0.001$) (Fig. 4E-H).

227 Thereafter, we separated the group in patients expressing low or high levels of IL-
228 6, based on the normative value for healthy individuals (upper 95th percentile reference
229 limit of healthy individuals: 4.45 pg/ml)³². Twenty-three DM1 patients out of 103 (22.3%)
230 had IL-6 levels over the reference limit of healthy individuals, suggesting that IL-6 is
231 abnormally elevated in this population (Fig. 4I). The average IL-6 level was 3.7-fold higher
232 ($p<0.001$) in the high IL-6 expressing group (7.61 pg/ml) compared to the low IL-6
233 expressing group (2.04 pg/ml). As expected, DM1 patients were weaker than normative
234 values for healthy individuals for most muscle groups even if their IL-6 level was low (Fig.
235 4J,K). However, the DM1 patients that express higher levels of IL-6 are significantly
236 weaker compared to those that had a normal SASP profile for all muscle groups tested:
237 ankle dorsiflexors (-18%, $p=0.006$), hip flexors (-14%, $p=0.001$), knee extensors (-12%,
238 $p=0.015$), knee flexors (-12%, $p=0.021$), shoulder flexors (-22%, $p=0.006$), shoulder
239 abductors (-16%, $p=0.016$), elbow flexors (-5%, $p=0.032$), elbow extensors (-24%,
240 $p=0.003$) (Figure 4J,K).

241 The functional capacity of DM1 participants was assessed using standardized
242 physical tests validated in the DM1 population: the Timed-Up and Go (time to rise from a
243 chair, walk 3 meters, walk back and sit down), 10-meter Walk-Test (10mWT; walking
244 speed over a short distance), Berg balance scale (14-item test assessing static and dynamic
245 balance), and pinch test (thumb to index pinch strength)^{33,34}. We observed a significant
246 correlation between IL-6 levels and the scores at the Timed-Up and Go (R: 0.400;
247 p<0.001), 10mWT (R: -0.388; p<0.001), Berg balance scale (R: -0.421; p<0.001), pinch
248 test (R: -0.345; p<0.001) (Fig. 4L,N,P,R). There was a significant reduction in the group
249 expressing higher levels of IL-6 compared to the one expressing lower levels of IL-6 in the
250 performance at the different functional tests: Timed-up and Go (+1 s [+10%], p=0.005), 10
251 mWT (-0.15 m/s [-12%], p=0.001), Berg balance scale (-4.1 [-7%], p=0.025), and pinch
252 test (-0.74 kg [-12%], p=0.032) (Fig. 4M,O,Q,S).

253 Further analysis using the stepwise regression model was used to verify if IL-6 is a
254 candidate predictor variable explaining muscle strength and functional outcomes. Results
255 show that IL-6, together with the clinical phenotype, age and/or sex of the patient, is a
256 variable that explain the variance of the scores obtained by participants to the Timed-up
257 and Go (standardized β: 0.18, p=0.048), 10mWT (standardized β: -0.2, p=0.003), Berg
258 balance scale (standardized β: -0.3, p=0.01), and the predicted maximal muscle strength of
259 hip flexors (standardized β: -0.27, p=0.02), knee extensors (standardized β: -0.20,
260 p=0.034), knee flexors (standardized β: -0.19, p=0.034), ankle dorsiflexors (standardized
261 β: -0.24, p=0.005), shoulder flexors (standardized β: -0.28, p=0.002), shoulder abductors
262 (standardized β: -0.22, p=0.009), elbow flexors (standardized β: -0.18, p=0.034), and elbow
263 extensors (standardized β: -0.206, p<0.001) (Suppl. table 4).

264 The same analyses were performed based on the serum level of TNF α . No
265 correlation was observed between TNF α levels and the strength of ankle dorsiflexors, hip
266 flexors, knee extensors, knee flexors, shoulder flexors, shoulder abductors, elbow flexors,
267 elbow extensors, 10mWT, and pinch test (suppl. Fig. 7). Only the Berg balance test (R:
268 0.269; p=0.006) and the Timed-up and go (R: -0.305; p=0.009) showed a mild correlation
269 with TNF α levels.

270 Altogether, our findings indicate that cellular senescence and SASP are hallmarks
271 of DM1, which could explain the reduced myogenic capacity and the impaired muscle
272 function. Therefore, we next explored the possibility of eliminating these senescent cells
273 as a potential therapy to alleviate DM1 disease progression.

274

275 **Senolytics specifically eliminate senescent myoblasts in DM1 and reduce SASP
276 expression**

277 Considering that the pathophysiological mechanism behind cellular senescence varies
278 depending on the inducers and cell types, we tested the impact of six different senolytics
279 that act through different mechanisms to induce apoptosis of senescent cells: the FOXO4-
280 DRI peptide (p53-FOXO4 interaction), Fisetin (PI3K/AKT pathway), Dasatinib +
281 Quercetin (PI3K/AKT pathway), Navitoclax (BCL-2/BCL-X inhibitor), A1331852 and
282 A1155463 (Selective BCL-X_L inhibitors)^{24,35-38}. Analysis of cell viability following the
283 treatment of myoblasts with different concentrations of senolytics showed that FOXO4-
284 DRI, Dasatinib + Quercetin, and fisetin were toxic for cells isolated from both healthy
285 controls and DM1 patients (Suppl. Fig. 8). Navitoclax selectively eliminated cells in DM1
286 samples at a specific concentration (3 μ m); however, A1155463 was the most effective to

287 target cells specifically in the DM1 group and not affect the healthy cell viability (Fig. 5A).
288 Moreover, A1155463 was effective at a lower concentration, in the nanomolar range.
289 Therefore, this lead compound was chosen for the following experiments. To confirm that
290 A1155463 induced apoptosis of senescent cells, an Annexin V/propidium iodide (PI) assay
291 was performed on healthy and DM1 myoblasts. Treatment of myoblasts with A1155463 at
292 a dose of 100 nM showed increased apoptosis only in the DM1 samples (Fig. 5B,C). SA-
293 β -Gal staining on DM1 or controls myoblasts treated with vehicle or A1155463 showed a
294 significant reduction in the number of SA- β -Gal+ senescent cells in the A1155463-treated
295 DM1 group (Fig. 5D,E). Further analysis of senescence genes expression demonstrated
296 that A1155463 treatment reduced *P16* expression in DM1 samples, but not in controls (Fig.
297 5F). The expression of SASP factors was analysed by multiplex Luminex assay in DM1
298 cells treated with A1155463 or vehicle. Results showed that senolytic treatment
299 significantly reduced the expression of many SASP factors such as CSF3 ($p=0.0005$),
300 CXCL1 ($p=0.018$), CXCL8 ($p=0.002$), CCL2 ($p=0.041$), MMP1 ($p=0.009$), and MMP3
301 ($p=0.027$) (Figure 5G). A trend toward reduction was also observed for IL-6 ($p=0.078$),
302 CCL7 ($p=0.054$), MMP2 ($p=0.06$), and MMP12 ($p=0.07$). On the other hand, growth
303 factors that stimulate cell proliferation such as EGF ($p=0.0005$) and FGF2 ($p=0.026$) were
304 increased by A1155463 treatment (Suppl. Fig 9). Other anti-inflammatory cytokines and
305 growth factors such as IL-4 ($p=0.28$), IL-13 ($p=0.13$), FLT-3L ($p=0.25$), and VEGF-A
306 ($p=0.38$) were not significantly affected by the treatment (Suppl. Fig. 9).

307

308 **The eradication of senescent cells restores myogenesis in DM1.**

309 Next, we aimed to determine if the elimination of senescent cells, and the associated
310 reduction in the expression of SASP factors, in A1155463-treated DM1 myoblasts restores
311 the myogenic potential of the non-senescent cells. Myoblasts were treated with A1155463
312 or vehicle for 1 day and were allowed to recover in proliferating media for 3 days.
313 Immunostaining for the proliferation marker KI67 revealed that A1155463-treatment
314 increased the proportion of KI67+ cells in the DM1 samples (1.8-fold increase), but not in
315 the controls (Fig. 6A-B). In another set of experiments, myoblasts were treated with
316 A1155463 or vehicle for 1 day and incubated in low serum differentiating medium for 5
317 days. Immunofluorescence staining for the differentiation marker MYOG revealed a
318 significant increase (2.2-fold) in the proportion of MYOG+ cells only in the DM1 samples,
319 and not in the controls (Fig. 6C-D). This increase in MYOG expression in the DM1 samples
320 was also confirmed by Western blot (Fig. 6E-F).

321 To better address the *in vivo* myogenic potential of DM1 myoblasts treated with
322 A1155163, we performed a cell transplantation assay. Three different DM1 myoblast lines
323 were treated with A1155463 (100 nM for 24 h) or vehicle and cells were allowed to recover
324 in proliferating media for 3 days. These cells were transplanted into the tibialis anterior
325 muscle of NSG mice that were injured by cardiotoxin (CTX) injection 1 day before.
326 Regenerated TA muscles were collected 21 days post-CTX injection (Fig. 6G). Cell
327 engraftment was assessed by co-immunolabeling for the human dystrophin protein
328 (hDMD) and total dystrophin protein (tDMD) (Fig. 6H). We observed that A1155463
329 enhanced DM1 cell engraftment by 50% when compared to vehicle (Fig. 6I). Taken
330 together these results indicate that A1155463 treatment can significantly improve the
331 myogenic potential of DM1 myoblasts *in vivo*.

332 **DISCUSSION**

333 Our findings demonstrate that cellular senescence is a hallmark of myogenic cells in DM1.
334 Using single cell transcriptomics and multiplex Luminex assay, we show that a subset of
335 these cells displays a molecular signature characterized by high levels of expression of
336 SASP factors. Our findings show that IL-6, a ubiquitous SASP factor, is associated with
337 muscle weakness and functional limitations in DM1 patients. By screening for different
338 senolytics, we identify a lead molecule, A1155463, that specifically eliminates senescent
339 cells in DM1. The senolytic-induced reduction of SASP is associated with a restoration of
340 the myogenic potential of DM1 myoblasts *in vitro* and *in vivo*. Altogether, these findings
341 provide novel insights on the physiopathology of DM1 and identify a new therapeutic
342 avenue for the treatment of this disease.

343

344 Signs of cellular senescence have been observed previously in cells isolated from skeletal
345 muscles of DM1 patients; however, these studies used a mixed population of cells that were
346 not purified by FACS and they did not validate if these senescence markers are co-
347 expressed with myogenic cell markers¹¹⁻¹³. Therefore, it was not possible to clearly
348 delineate if myogenic cells, or if fibroblasts for instance, were becoming senescent.
349 Particularly, fibroblasts or mesenchymal stromal cells are a predominant senescent cell
350 type in various pathogenic conditions³⁹. Here, we use FACS purified myogenic cells and
351 we have confirmed that senescence markers (e.g., P16) are expressed in DM1 purified
352 myoblasts. Moreover, co-staining for P16 positive cells and PAX7 on skeletal muscle
353 biopsies revealed the presence of senescent muscle stem cells *in situ*, which has never been
354 described before. These findings indicate that cellular senescence in DM1 is not only an *in*

355 *vitro* artefact caused by replicative stress, but a relevant pathophysiological process of the
356 disease. Furthermore, our experiments were performed on samples from individuals with
357 the infantile, juvenile or adult form of the disease, while previous studies focused
358 exclusively on the more severe congenital form, suggesting that cellular senescence is a
359 hallmark of the disease no matter the clinical form^{12,40}.

360

361 Our findings show that the accumulation of RNA foci in the nuclei of DM myoblasts is
362 associated with cellular senescence, suggesting that RNA-mediated toxicity is the cause
363 of senescence in this disease. Toxic RNA accumulation caused by the CTG repeats in the
364 *DMPK* gene is known to induce reactive oxygen species (ROS) production and oxidative
365 damage in DM1^{14,41-44}. Chronic ROS production triggers a DNA damage response leading
366 to cell cycle arrest and cellular senescence, which in turn secretes further ROS and SASP
367 leading to a feed-forward cycle^{14,45,46}. Using C2C12 cells it was shown that the insertion
368 of CUG repeats increases ROS production, which is further exacerbated by H₂O₂ exposure,
369 suggesting that DM1 cells produce more ROS and are more sensitive to oxidative stress¹⁴.
370 Analysis of the GO enrichment data of our single cell transcriptomic dataset show that the
371 most dysregulated genes in DM1 patients' cells are involved in oxidative phosphorylation.
372 Moreover, pathway analysis also shows an enrichment for genes related to ROS and
373 reactive nitrogen species (RNS) production. Analyses from other datasets also show an
374 increase in ROS producing genes (e.g., *NOX4*) and a decrease in antioxidant genes (e.g.
375 *SOD3*)^{14,47}. Notably, the expression of antioxidant genes such as *SOD1*, *SOD2*, and *GPX1*
376 have been positively associated with muscle strength in another DM1 transcriptomic
377 dataset, suggesting that antioxidant levels could help protect against senescence-associated

378 muscle wasting⁴⁸. Overall, our findings and others suggest that senescence in DM1
379 myoblasts is induced by toxic RNA-mediated oxidative stress.

380

381 Other transcriptomics datasets have been generated on DM1 tissues and cells (reviewed in
382 ⁴⁹). A study on DM1 myogenic cells showed that the transcriptional changes are more
383 important in DM1 myoblasts than myotubes⁴⁷. GO term analysis showed that the biological
384 processes that are mostly enriched in DM1 myoblasts are signalling pathways, ECM
385 components, and cytoskeletal organisation⁴⁷. Another RNAseq dataset performed on
386 human embryonic stem cells (DM1 and controls) differentiated into myogenic cells showed
387 that inflammatory pathways such as IL6-JAK-STAT3 signalling are overexpressed in DM1
388 cells, which is coherent with the inflammatory signature that we observed⁵⁰. Similarly,
389 RNAseq analysis performed on isogenic myoblasts containing or not a CTG₂₆₀₀ expansion
390 showed an enrichment in biological processes such as cellular response to IFN γ ⁵¹. Using a
391 model of C2C12 cells containing expanded CUG repeats, it was also shown that toxic RNA
392 expression induces a senescence-like signature characterized by enrichment in genes
393 related to ECM organisation, response to oxygen levels, apoptosis, and regulation of cell
394 growth¹⁴. Transcriptomic analysis on skeletal muscle samples from individuals with the
395 congenital form of DM1 showed a signature very similar to our scRNAseq dataset
396 characterized by downregulation in myogenesis genes and upregulation in inflammatory
397 genes, such as the IL6/STAT3 target genes *SAA1* and *SAA2*⁴⁰. Moreover, supporting our
398 results, RNAseq on muscle samples from DM1 patients and controls showed that genes
399 related to SASP factors (e.g. *CXCL14*, *CXCL16*, and *MMP2*) or cell cycle inhibitors (e.g.
400 *CDKN1A*, *TP63*)⁵², are negatively correlated with muscle strength in DM1⁴⁸. RNAseq

401 performed in other tissues such as the frontal cortex showed an enrichment in inflammatory
402 genes compared to healthy individuals, suggesting that the pro-inflammatory signature is
403 a common feature in different DM1 tissues⁵³. These findings bring important insights on
404 the molecular mechanisms in DM1, however, bulk RNAseq analysis limits the
405 interpretations regarding the subpopulation of cells affected. Particularly, it is not possible
406 with these datasets to determine if the inflammatory signature is generalized or
407 circumscribed to a specific subset of cells, which is especially important in the context of
408 cellular senescence.

409

410 To assess the specific molecular signature of myogenic cells in DM1, we used an
411 unbiased approach through scRNAseq. This is the first single cell transcriptomics dataset
412 generated in DM1⁴⁹. This dataset allowed to identify specific cell clusters expressing
413 different levels of senescence markers leading to a better comprehension of the different
414 stages of senescence in myoblasts of patients with DM1. Particularly, we identified a
415 specific cluster of DM1 myoblasts expressing high levels of SASP factors, while another
416 cluster expressed higher levels of *SAA1* and *SAA2*, two molecules that are triggered by
417 SASP factors and can further stimulate SASP expression by a positive feedback loop^{27,54}.
418 These findings suggest that the expression of SASP by senescent cells have paracrine
419 effects on neighbouring cells and promote their senescence-like phenotype. Moreover, this
420 dataset identified that, while a subset of cells shows a fully senescent or early senescent
421 profile, there is a significant proportion of cells that had a similar molecular profile as the
422 one found in our control samples from healthy individuals. These results suggest that
423 elimination of the senescent myoblasts could restore the myogenic activity of non-

424 senescent DM1 myoblasts. Several studies used this approach to alleviate chronic and
425 degenerative diseases in which senescence contributes to the progression of the disease
426 (reviewed in^{55,56}). By testing different senolytic drugs, we observed that DM1 senescent
427 myoblasts were particularly responsive to inhibitors targeting the BCL family members.
428 Navitoclax (ABT-263; BCL2/BCL-XL inhibitor) was effective at targeting senescent
429 myoblasts in DM1, similar to what was shown in an aging model³⁸; however, the highest
430 efficiency was achieved with the BCL-XL inhibitor A1155463. Notably, our SCENIC
431 analysis showed an enrichment in the activity of the transcription factors of the NF- κ B
432 family, which are known to bind to promoter region of Bcl-xl gene to stimulate its
433 expression⁵⁷. Other widely used senolytic such as FOXO4-DRI, fisetin, or dasatinib +
434 quercetin that affect other pathways were ineffective to specifically target senescent DM1
435 myoblasts^{24,36}, which indicate that the senescent molecular signature expressed in DM1
436 myoblasts is distinct to this cell type/inducer and that specific molecular targeting is
437 necessary to eliminate these cells.

438

439 Our findings demonstrate that IL-6, a main component of the SASP cocktail, is
440 correlated with muscle weakness and functional capacity limitations in DM1. These results
441 are consistent with previous observations showing that members of the IL-6 signalling
442 pathway are correlated with signs of histological degenerative changes in the congenital
443 form of the disease⁴⁰. On the other hand, our findings show that another pro-inflammatory
444 cytokine, TNF α , was not correlated with muscle weakness. These results are consistent
445 with our scRNAseq data showing an increase in the expression of *IL6* but not *TNF* in
446 samples from DM1 patients. These results suggest that there is a specific SASP signature

447 associated with muscle weakness in DM1, and not only a generalized pro-inflammatory
448 profile. Similarly, another study screened for 20 pro-inflammatory cytokines in the serum
449 of patients affected by facioscapulohumeral muscular dystrophy and identified IL-6 as the
450 only cytokine correlating with muscle weakness and disease severity⁵⁸. These findings
451 suggest that IL-6 is a promising biomarker to determine the severity of muscle dysfunction
452 in DM1⁵⁹.

453

454 Our results also suggest that targeting SASP cytokines such as IL-6 is a valid
455 therapeutic approach to mitigate disease progression. Our findings showed that specific
456 elimination of senescent DM1 myoblasts leads to a reduction in the expression of SASP
457 molecules, which restores the myogenic function of non-senescent DM1 myoblasts
458 through an improvement of their cellular proliferation and differentiation capacity. These
459 results are consistent with a previous study showing that the secretion of SASP by
460 senescent cells block myoblast differentiation *in vitro*⁶⁰. The improvement in myogenesis
461 was not observed in cells from healthy individuals, which confirms that the senolytic drug
462 targets a specific pathophysiological mechanism in DM1.

463

464 Overall, this study describes a well-defined senescent molecular signature in DM1
465 myogenic cells, which brings novel insights on the pathophysiological mechanisms of the
466 disease. Particularly, it identifies the production of SASP as a major characteristic of DM1
467 myoblasts, which is associated with muscle weakness in DM1. We demonstrated that
468 specific drugs can be used to target these defective cells and restore myogenesis. These
469 findings open a new therapeutic avenue that could help to mitigate the impact of DM1, a
470 disease for which no treatment currently exists to slow symptoms progression⁶¹.

471

472 **METHODS**

473

474 **Participants' recruitment**

475 Patients were recruited at the Saguenay Neuromuscular Clinic of Jonquière (Québec,
476 Canada) and healthy individuals were recruited among the friends/family members or team
477 members. Inclusion criteria for DM1 participants were to be aged over 18-year-old and
478 have a genetically confirmed diagnosis of DM1. One hundred and three DM1 participants
479 were recruited between 2002-2004 and completed muscle and functional capacity
480 assessments and blood sample collection. Ten DM1 patients and seven healthy individuals
481 were recruited in 2019 and undergone a muscle biopsy only. This study was approved by
482 the Ethics review board of the Centre de santé et de services sociaux de Chicoutimi,
483 Canada. Written informed consent was obtained from all participants.

484

485 **Muscle strength, functional capacity assessments, and blood sample collection**

486 A blood sample was taken from each participant and the level of IL-6 was measured at the
487 *Centre de recherche sur les maladies lipidiques* of the *Centre hospitalier de l'Université*
488 *Laval* (Québec, Canada). DM1 patients were classified in a low or high IL-6 expressing
489 group based on the cut-off value representing the upper 95th percentile value for healthy
490 individuals (4.45 pg/ml)³². The maximum isometric muscle strength of the ankle
491 dorsiflexors, hip flexors, knee flexors, knee extensors, shoulder flexors, shoulder
492 abductors, elbow flexors and elbow extensors was assessed using quantitative muscle
493 testing according to a standardized protocol⁶². Muscle strength was expressed as the

494 expected muscle strength of healthy individuals based on a French isometric strength
495 normative database using predictive equations taking into consideration age, sex, and
496 weight of the patients³¹. Patients were subjected to a battery of validated functional
497 tests^{63,64}. Timed-up and Go: time to stand up, walk three meters, turn and walk back to sit
498 down on the chair; 10mWT: comfortable walking speed (m/s) along a 10-meter distance;
499 Berg balance scale: 14 items measuring static and dynamic balance (maximum score of 56
500 indicating no deficit in balance); Pinch strength: measured using a B&L pinch gauge (kg).
501 All tests were conducted under the supervision of a trained physiotherapist
502

503 **Muscle biopsy**

504 A biopsy of the vastus lateralis at the mid-thigh level was taken using the modified
505 Bergstrom needle technique with suction⁶⁵. A ~200 mg sample of muscle was obtained,
506 rinsed in sterile phosphate buffered saline solution (PBS) and portioned out for the various
507 following analyses. The first half of the sample (approximately 100 mg) was kept in sterile
508 SK-MAX media (Wisent Bio) on ice for muscle stem cell isolation. The second half of the
509 muscle sample was separated in two parts that were flash frozen for qPCR analysis (50 mg)
510 or embedded in OCT tissue freezing medium and frozen in 2-methylbutane cooled in
511 liquid nitrogen (50 mg). The samples were stored at -80°C.
512

513 **Myogenic cell lines isolation, purification, and culture**

514 Muscle biopsies from controls and patients were minced, digested in collagenase, and
515 plated in a culture dish⁶⁶. Myoblasts were grown in Sk-MAX media complemented with
516 Sk-MAX supplement and 20% fetal bovine serum (FBS). Myoblasts were expanded for a

517 few days until there were enough cells for purification by FACS. Myoblasts were stained
518 with 7-AAD (cell viability) and with the positive selection marker anti-CD56 AF647-
519 conjugated (clone R19-760, BD biosciences). Of note, preliminary experiments showed
520 that virtually all CD56+ cells were also positive for another myogenic marker CD82 (data
521 not shown)⁶⁷, and therefore only CD56 was used for the follow-up experiments. Myoblasts
522 differentiation was induced by exposing cells to 2% horse serum (HS) in DMEM media.
523 Control and DM1 myoblasts were used for experiments at the same low passage (maximum
524 P6).

525

526 Single-cell RNA-sequencing experiments

527 Single cell suspensions of myogenic cells were resuspended in PBS containing 0.04%
528 ultra-pure BSA. scRNAseq libraries were prepared using the Chromium Single Cell 30
529 Reagent Kits v3.1 (10x Genomics; Pleasanton, CA, USA) according to the manufacturer's
530 instructions⁶⁸. Generated libraries were sequenced on an Illumina HiSeq4000.

531 Raw sequencing data were preprocessed using Cell Ranger 6.1.2⁶⁹ to perform the
532 alignment (human genome GRCh38- 2020-A), filtering, barcode counting, and UMI
533 counting at a single cell resolution, generating a control, patient, and a merged digital gene
534 expression (DGE) matrix containing 1,902, 2,029 and 3,931 cells respectively. Further
535 downstream analyses were conducted using R package Seurat v4.0 (spatial reconstruction
536 of single-cell gene expression data⁷⁰) and singleCellTK v2.2.0 (Single cell Toolkit).

537 Quality control: Due to deep sequencing of the libraries, for each DGE matrix, cells
538 expressing fewer than 1,000 genes and more than 10% of mitochondrial genes were filtered
539 out, leaving a total of 3,381 cells in the merged matrix (1,639 cells from controls and 1,742

540 cells from patients). For all cells, genes were excluded if they were expressed in less than
541 3 cells. We normalized the DGE matrices by the total number of UMIs in each cell and
542 scaled by 10^6 to yield counts per million (CPM). We natural log transformed these matrices
543 after the addition of a pseudocount of 1 to avoid undefined values.

544 The 2,000 most variable genes were selected for each DGE matrix, based on their
545 relative dispersion (variance/mean) regarding to the expected value across genes with
546 similar average expression⁷¹. Next, we performed a linear transformation ('scaling') to
547 each matrix to minimize variations due to technical noise or possible batch effects.

548 We used DoubletFinder⁷² to identify putative doublets in each DGE matrix relying
549 solely on gene expression data. DoubletFinder requires three input parameters for the
550 doublet classification: the number of expected real doublets (nExp), the number of artificial
551 doublets (pN) and the neighborhood size (pK). We calculated the nExp by multiplying the
552 number of cells by the expected doublet ratio (1.6%) based on 10x genomics Chromium
553 user guide. To identify pN and pK values, we performed the parameter optimization of
554 DoubletFinder resulting in a pN of 0.30 for all matrices and a pK of 0.24, 0.01 and 0.005
555 for the control, patient, and merged matrices respectively. After the removal of putative
556 doublets, we remain with 1,613 cells in the control, 1,714 cells in the patient, and 3,327
557 cells in the merged matrix for downstream analyses.

558 We estimated cell cycle activity by scoring the expression of a set of S phase–
559 associated and G2/M phase–associated genes, as implemented in Seurat⁷⁰.

560 To enable unsupervised clustering, we performed a linear dimensionality reduction
561 with principal component analysis (PCA) on each DGE matrix using the highly variable
562 genes previously identified. Once embedded in this PCA space, we applied a K-nearest

563 neighbor (KNN) graph-based clustering approach and refine the edge weights between any
564 two cells based on the shared overlap in their local neighborhoods, identifying the k = 10
565 nearest neighbors for each cell. To cluster the cells, we apply a Louvain algorithm⁷³ to
566 iteratively group cells together, with the goal of optimizing the standard modularity
567 function. A resolution of 0.3 was used in the patient matrix to identify more defined cell
568 populations. The t-Distributed Stochastic Neighbor Embedding (tSNE)⁷⁴ and the Uniform
569 Manifold Approximation and Projection (UMAP) were used to visualize the clustering
570 results; however, UMAP was chosen because it provides a better separation of the groups.

571 We computed differentially expressed genes (DEGs) between controls and patients
572 using the Wilcoxon rank-sum test with the Benjamini-Hochberg procedure for FDR
573 control⁷⁵, identifying positive and negative markers for each group. DEGs with $|\log FC| >$
574 1.0 and adjusted p-values $< 10e-6$ were considered. In addition, we also computed the
575 proportion and the probability distribution of cells expressing each gene in each group.
576 To identify DEGs among patient clusters and patient cells after the senescence annotation
577 (method described below), we used the model-based analysis of single-cell transcriptomics
578 method (MAST)⁷⁶. DEGs with $|\log FC| > 0.25$, FDR < 0.05 , percentage cluster expression $>$
579 0.5, percentage expression in the control group < 0.4 , and adjusted p-values < 0.01 were
580 considered. For the senescent and non-senescent populations, DEGs with an adjusted p-
581 values < 0.01 and $\log FC > 1.5$ in one condition and $\log FC < 1.5$ in the other condition were
582 plotted regardless the expression of the control.

583 Gene Ontology terms were analyzed for DEGs identified in each cell type using the
584 online Metascape tool (<https://metascape.org>)⁷⁷ with default parameters: Min Overlap = 3,
585 p-value Cut-off = 0.05, and Min Enrichment = 1.5. The top 20 terms ranked by p-value

586 were displayed in a bar diagram. Pathway enrichment analysis was performed using R
587 package ReactomePA v1.36.0 and displayed in a bubble diagram⁷⁸.

588 To perform the annotation of senescent and non-senescent cells in patient cells, we
589 used the R package GSVA v1.40.1⁷⁹ to compare the average expression of the DEGs of
590 each patient cluster with reference gene sets related to cellular senescence and secretory
591 processes^{28,80-82}. Heatmap and density plots are displayed. Clusters with GSVA scores > 0
592 in all gene sets were annotated as fully senescent cells, clusters with GSVA scores < 0 in
593 all gene sets were annotated as non-senescent cells, and clusters with positive and negative
594 GRVA values were annotated as early senescent cells.

595
596 **Senescence associated beta-galactosidase staining**

597 CellEvent, senescence green detection kit (ThermoFisher, C10850) was used to label
598 senescent cells according to the manufacturer's specifications. The fluorescent probe
599 included in the assay is a substrate for beta-galactosidase and emits a 488 AlexaFluor
600 fluorogenic signal in cells containing the beta-galactosidase active enzyme.

601

602 **Fluorescence in situ hybridization (FISH)**

603 Following the SA-β-gal staining protocol, cells were fixed with 2% PFA solution for 10
604 min at room temperature, washed, and dehydrated in prechilled 70% ethanol for 3 h at 4°C.
605 Thereafter, cells were washed in PBS RNase free for 10 min, incubated in 40% formamide
606 (Millipore, Ca) in 2× saline-sodium citrate (SCC) buffer (300 mM sodium chloride, 30 mM
607 sodium citrate, pH 7.0) for 10 min at room temperature, and blocked in hybridization buffer
608 (40% formamide, 2× SCC buffer, 200µg/mL bovine serum albumin, 100 mg/mL dextran
609 sulfate, 2 mM vanadyl sulfate, 1 mg/mL yeast tRNA) for 15 min at 37°C⁸³. The Cy5-

610 labeled (CAG)10 DNA probe was denatured for 10 min at 100°C, chilled on ice for 10 min,
611 then added to prechilled hybridization buffer for a final concentration of 150 ng/µL probe.
612 Cells were incubated with the probe for 2 h at 37°C. As a negative control, RNase solution
613 were incubated for 10 min at RT before the hybridization of the probe. Cells were washed,
614 counterstained with DAPI, and images were acquired on SP8 confocal microscope (Leica).

615

616

617 **RT-qPCR**

618 Myogenic cells total RNA was extracted with Qiazol reagent according to the
619 manufacturer's specifications. Total RNA was quantified with a Thermo Scientific™
620 NanoDrop™ 8000 Spectrophotometer. Reverse transcription was performed on 1 µg of
621 total RNA using the RT mastermix (QuantiTect Reverse Transcription Kit, 205313) to
622 obtain cDNA. qPCR was performed with a set of primers designed on Primer-BLAST
623 (NCBI) and validated for their specificity, efficiency and annealing temperature⁸⁴. Gene
624 amplification was performed with the BlasTaq™ 2X qPCR MasterMix (Abm, G892) on a
625 Roche LightCycler® 480 Instrument II. Data were analysed with the LightCycler® 480
626 and were normalised relative to RPLPO expression⁸⁵. The primers used are shown in
627 Supplemental Table 5.

628

629 **Immunofluorescence**

630 Muscle biopsies were cut at 10 µm thick in using a NX50 Cryostar (Thermo). Slices were
631 put on positively charged Superfrost slides. Immunostaining was performed on skeletal
632 muscle sections or on primary myoblast cultured on plastic dishes. Samples were fixed

633 with 2% PFA for 5 min (sections) or 10 min (cells). Sections were incubated with a
634 blocking solution containing 5% of donkey serum and 2% of bovine serum albumin (BSA)
635 in PBS for 60 minutes at room temperature. Sections were incubated overnight at 4°C with
636 the following primary antibodies diluted in blocking solution: PAX7 (clone PAX7, 1:20;
637 Developmental Studies Hybridoma Bank, DSHB), P16 (ab54210, 1:50; Abcam), P21
638 (clone F5, sc-6246, 1:50; Santa Cruz), KI67 (14-5698-82, 1:500; Invitrogen), MYOG
639 (ab124800, 1:200; Abcam), hDMD (MANDYS106(2c6), 1:2; Developmental Studies
640 Hybridoma Bank, DSHB), total DMD (ab15277, 1:200; Abcam). Secondary antibodies
641 were also diluted in blocking buffer (1:1,000) and incubated for 1 h at room temperature.
642 Secondary antibodies (Invitrogen) used were donkey anti-mouse 488 (A21202) or donkey
643 anti-mouse 594 (A21203), donkey anti-rabbit 488 (A21206) or donkey anti-rabbit 647
644 (A32795). Slides were mounted using PermaFluor mounting medium (Fisher Scientific).
645 Immunofluorescence pictures of samples were taken with EVOS M5000 (Thermo Fisher
646 Scientific) or Leica TCS SP8 DLS confocal microscope. Pictures were analyzed using
647 ImageJ software (version 1.53, National Institutes of Health, USA).

648

649 **Viability assay**

650 Cell viability was determined by Cell-titer 96 aqueous one solution cell proliferation assay
651 kit (Promega, G3580) according to the manufacturer's specifications. Briefly, aliquots of
652 5×10^3 cells/well were cultured in 96-well plates. After 24 hours in culture, cells were
653 treated with vehicle (DMSO) or the following senolytics: FOXO4-DRI (NovoPro), Fisetin
654 (Selleck chemicals), Dasatinib + Quercetin (Sigma), Navitoclax (ABT-263, Abcam),
655 A1331852 (Selleck Chemicals), or A1155463 (Selleck Chemicals), at different

656 concentrations for 48 h. Then, 40 µl of Cell-titer 96 aqueous one solution was added to
657 each well and incubated for an additional 3 h. The absorbance at 490 nm was recorded with
658 a 96-well plate reader (BMG Labtech, CLARIOstar).

659

660 **Apoptosis assay**

661 Apoptotic cells were identified using a detection kit (Biolegend, FITC Annexin V
662 Apoptosis Detection Kit with PI, 640914) according to manufacturer's specifications. After
663 trypsinization, cells were washed twice with Cell Staining Buffer and stained with FITC
664 Annexin V (1:30) and PI (1:10) for 15 minutes at room temperature. Then, 400 µl of
665 Annexin V binding buffer was added, and the samples were analyzed by LSR Fortessa
666 cytometer (BD Biosciences).

667

668 **SASP markers Luminex assay**

669 A multiplex Luminex assay (Eve Technologies, Calgary, Alberta) was used to measure
670 SASP markers of myogenic cells supernatant media. Two different discovery assays were
671 chosen to assess SASP markers: Human Cytokine/Chemokine 48-Plex Discovery Assay®
672 Array (HD48) and Human MMP and TIMP Discovery Assay® Array. Cells were treated
673 with senolytic or vehicle and incubated for 36 hours. Cell media was changed, and cells
674 were incubated for another 36 hours before supernatant collection. Supernatants were
675 stored at -80 °C until assayed.

676

677 **Western blot**

678 Cells were washed with sterile PBS and lysed with ice-cold RIPA buffer containing 1% of
679 protease inhibitors and centrifuged at 10,000 g for 10 min. The supernatant was retained,
680 aliquoted, and the protein content was quantified using the BCA Assay Kit (Thermo
681 scientific, Mississauga, Ontario, Canada). A volume corresponding to 40 µg of protein was
682 diluted with a sample buffer (125 mM Tris buffer (pH 6.8), 4% SDS, 20% glycerol, 0.05%
683 bromophenol blue, and 200mM dithiothreitol), heated at 100°C for 5 min and
684 electroseparated on 15% sodium dodecyl sulfate-polyacrylamide gel. Proteins were
685 transferred to polyvinylidene difluoride membranes, which were blocked with 5% non-fat
686 milk or 5% BSA for 90 min at room temperature. Membranes were immunoblotted
687 overnight at 4°C with anti-myogenin (ab124800, 1:500; Abcam) and anti-beta-actin
688 (4967S, 1:5,000; Cell Signaling) as primary antibodies. After washing, membranes were
689 incubated with goat anti-rabbit (H+L) HRP-conjugated secondary antibodies (1:5,000;
690 Abcam, ab6721) for 1 h at room temperature. Bands were revealed with ECL-plus Western
691 blotting reagent (PerkinElmer Life and Analytical Sciences, USA), visualized with the
692 BioRad ChemiDoc Imaging System, and quantified using ImageJ (National Institutes of
693 Health, Maryland, USA). Densities were normalized to the loading control.

694

695 **Cell transplantation assay**

696 NOD/SCID/IL2R γ null (NSG) mice were housed in the animal care facility at the CHU
697 Sainte-Justine Research Center under pathogen-free conditions in sterile ventilated racks.
698 All *in vivo* manipulations were previously approved by the institutional committee for good
699 laboratory practices for animal research (protocol #2020-2357). To induce muscle
700 regeneration and enhance cellular engraftment, a cardiotoxin injection (Latoxan, 50 µl of

701 10 µM solution in saline) was performed intramuscularly (i.m.) through the skin in the right
702 and left tibialis anterior (TA) muscles under general anesthesia. After 24 hours, 2×10^5
703 DM1 myoblasts (resuspended in 10 µl of PBS) that were previously treated with A1155463
704 or vehicle for 72 hours were transplanted into the right or left injured TA muscle,
705 respectively. Three different cell lines were used, and each cell line was transplanted into
706 3 different mice. Mice were allowed to recover for 20 days after which they were
707 euthanized by CO₂ inhalation (under anesthesia) followed by cervical dislocation and their
708 TA muscles were collected. Tissues were embedded in OCT tissue freezing medium and
709 frozen in 2-methylbutane cooled in liquid nitrogen and stored at -80°C until sectioning.

710

711 Statistical analysis

712 Sample size determination was based on the expected effect size and variability that was
713 previously published for similar readouts using DM1 patient myogenic cultures^{5,12}. No data
714 were excluded. All experiments were repeated independently at least twice in the
715 laboratory with similar results. For each set of experiments, the proportion of control and
716 DM1 patients were matched as best as possible for age and sex. For data collection and
717 analysis, the experimenter was blinded to the identity of the sample. For *in vitro*
718 experiments, data were analyzed with the MIXED procedure of the Statistical Analysis
719 System (SAS Institute, version 9.2, Cary, North Carolina, USA). Normality was verified
720 for all data according to the Shapiro–Wilk test. Treatment effects were determined with
721 two-tailed Student’s t-tests, One-way or Two-way analysis of variance (ANOVA)
722 uncorrected Fisher’s Least Significant Difference (LSD) test. Results are reported as mean
723 ± standard error of the mean (SEM). For *in vivo* data analyses, associations between IL-6

724 level and muscle strength and functional capacity of patients were assessed using Spearman
725 ρ correlation coefficient. Comparisons of muscle strength and functional capacity between
726 patients based on IL-6 normative value for healthy individuals (below or over the
727 threshold) were performed using Mann-Whitney U Test. Stepwise multiple regression
728 analyses were used to determine which variables among age, sex, phenotype and IL-6 level
729 (low or high) best explain each variable of muscle strength and functional capacity. For all
730 tests, the significance value was set at p -value $<.05$. Data were analyzed using IBM SPSS
731 Statistics for Windows, Version 24.0 (Armonk, NY: IBM Corp).

732

733

734 **ACKNOWLEDGEMENTS**

735 We thank M. M. Hicham Affia, Ms. Veronique Lisi, and Ms. Lydia Tellier for their
736 technical assistance. T.C.C. was supported by a fellowship from the Myotonic Dystrophy
737 Foundation. G.D.B. was supported by CHU Sainte-Justine, University of Montreal, and
738 RQR (réseau québécois en reproduction) awards. Z.O. was supported by an award from
739 the MITACS fellowship. I.M. was supported by CERMO-FC (Center of Excellence in
740 Research on Orphan Diseases – Fondation Courtois) and TheCell awards. A.D. was
741 supported by an FQRNT (Fonds Québécois de la recherche - nature et les technologies)
742 doctoral award. M.P.R. was supported by an FRQS (Fonds Québécois de la recherche –
743 Santé) doctoral award. G.A. holds the Banque Nationale Research Excellence Chair in
744 Cardiovascular Genetics. E.D. was supported by FRQS Junior-1 award and N.A.D. and
745 S.M. were supported by FRQS Junior-2 award. This study was supported by grants from
746 Canadian Institutes of Health Research (CIHR) (grant no. MOP-49556, JNM-108412), the

747 Quebec Cell, Tissue and Gene Therapy Network –ThéCell (a thematic network supported
748 by the FRQS) and Muscular Dystrophy Canada.

749

750 **AUTHOR CONTRIBUTIONS**

751 N.A.D. and E.D. conceived and managed the project. T.C.C, G.D.B, Z.O., I.M., M.P.R,
752 A.D., O.P., D.M., I.C., B.B., S.L., J.M., C.G. designed and performed experiments, and
753 collected data. J.M., C.G., G.A., C.B., S.M, T.C.C, L.F., G.D.B, I.C., E.D. and N.A.D.
754 analyzed and interpreted the data. T.C.C, G.D.B, E.D., and N.A.D wrote the manuscript.

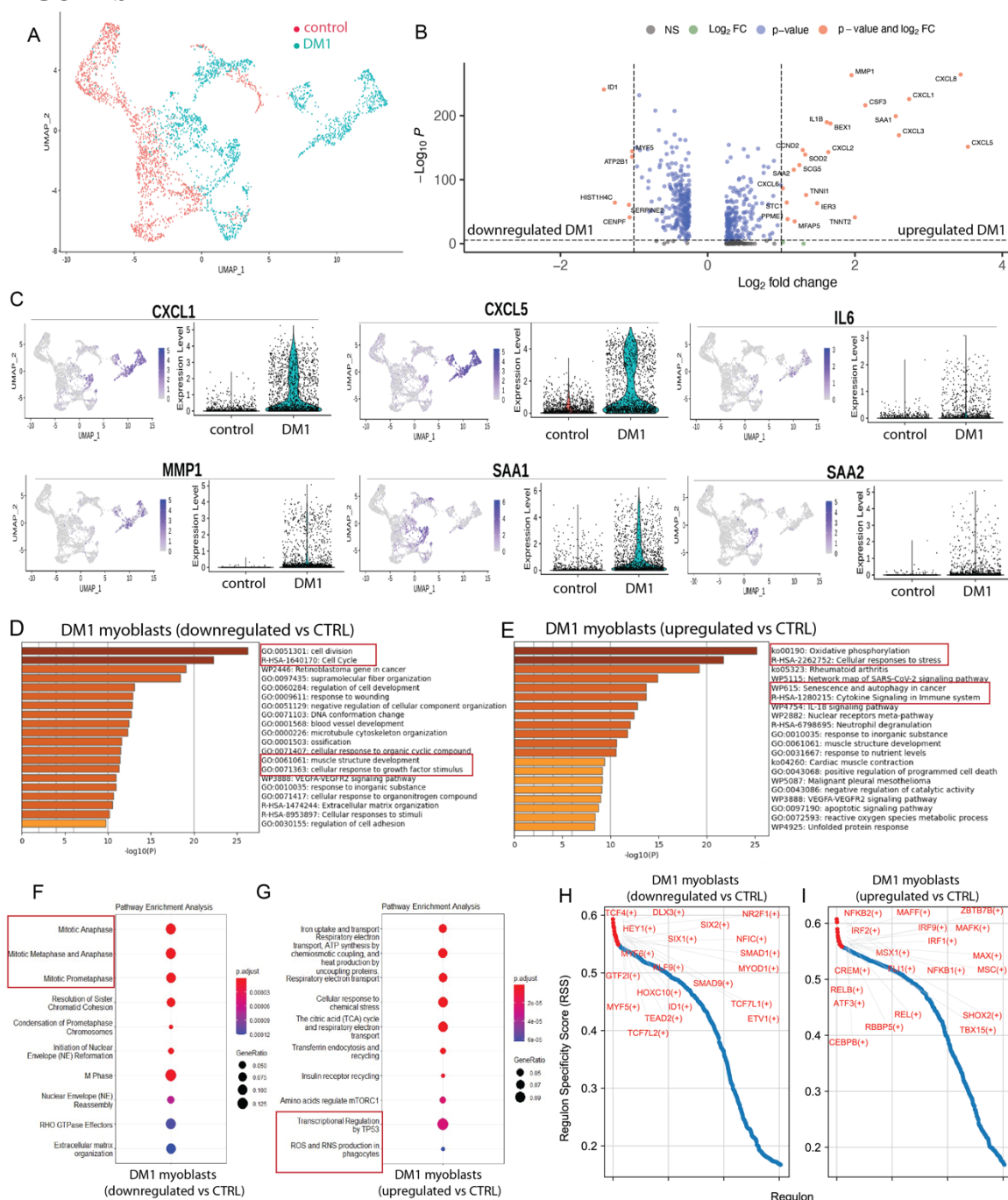
755 All authors carefully reviewed and provided critical insights to the manuscript.

756

757 **COMPETING INTERESTS**

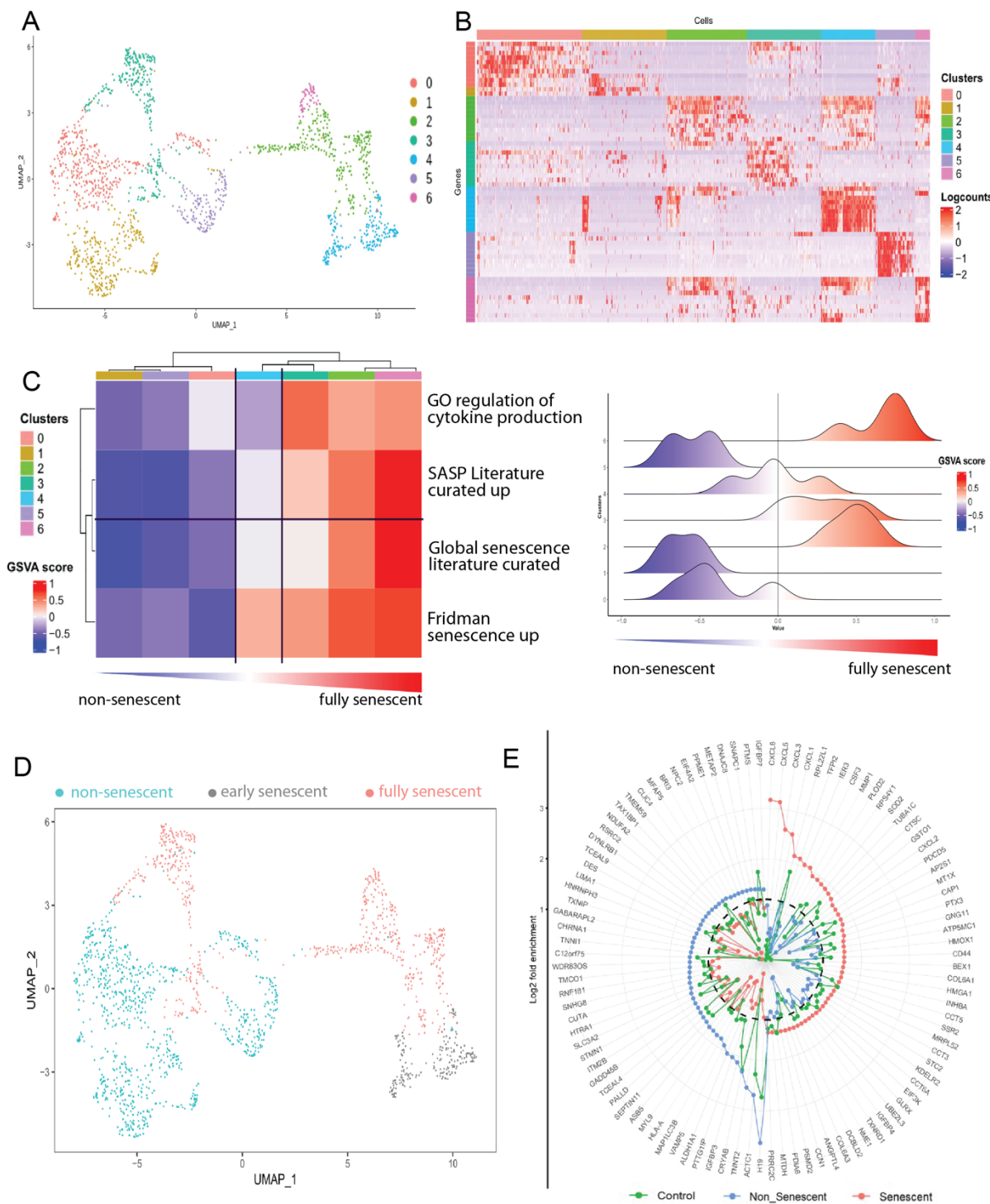
758 The authors have declared that they have no conflict of interest

759 **FIGURES**



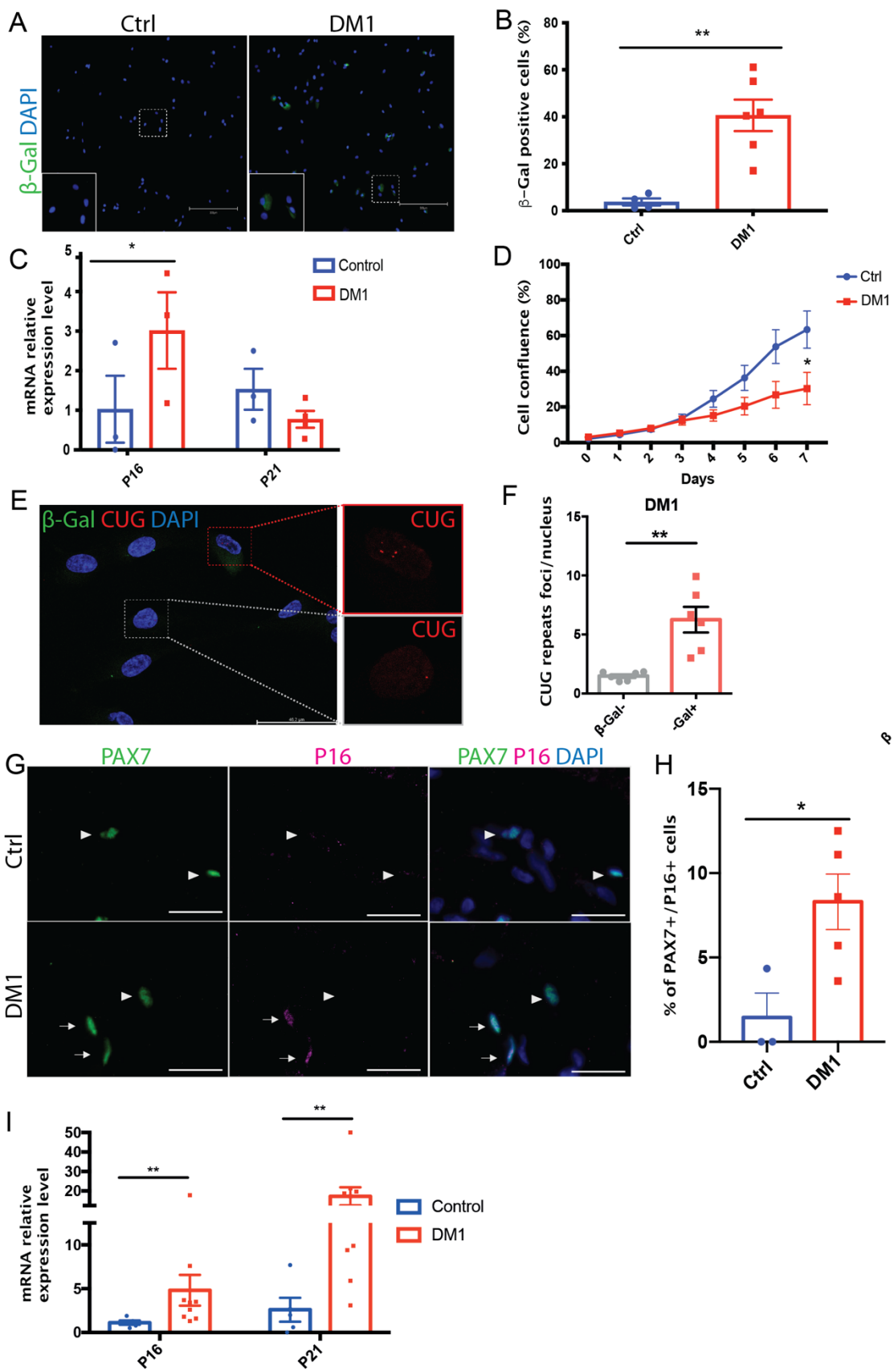
769 top DEGs ($|\log_{2}\text{FC}| > 1.0$; vertical dotted line). **C**) Feature and violin plots showing the
770 expression of selected DEGs in DM1 patient and control cells. **D,E)** Functional enrichment
771 analysis with GO Biological Processes analysis using DEGs downregulated (**D**) and
772 upregulated (**E**) in DM1 vs control (CTRL) cells. The X-axis represents the $-\log_{10}(\text{P}-$
773 value). **F,G)** Bubble diagram showing the top 10 Reactome pathways for DEGs
774 downregulated (**F**) and upregulated (**G**) in DM1 vs control cells. Vertical axes show
775 enriched terms, and horizontal axes represent the genes in each cluster. Larger node size
776 represents the larger ratio of enriched genes/total genes. **H,I)** Rank for regulons for
777 downregulated genes (**H**) or upregulated genes (**I**) in DM1 vs control cells based on regulon
778 specificity score (RSS).

779



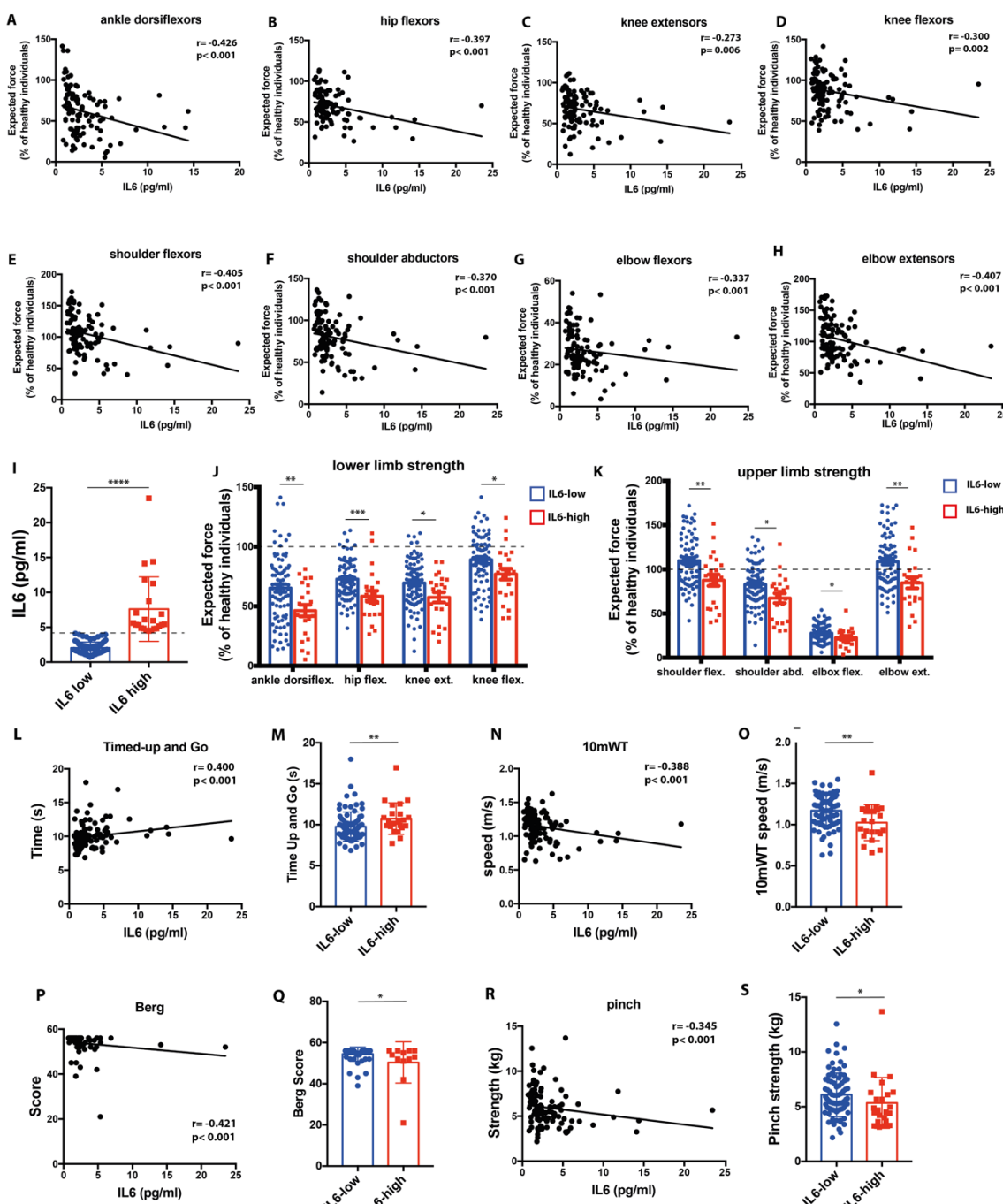
780
 781 **Figure 2: Identification of senescent cell subpopulations in patients with DM1.** A)
 782 UMAP visualization showing unsupervised clustering revealing 7 distinct cell populations
 783 in patient cells. B) Heatmap showing the top differentially expressed genes (DEGs) from
 784 each cluster. C) Heatmap and ridge plots showing the fold change of GSVA score on gene
 785 sets related to cellular senescence and cytokine secretion comparing DEGs transcripts from
 786 each cluster. Clusters with positive GSVA values for all the gene sets were annotated as

787 fully senescent while clusters with mixed and negative GSVA scores were annotated as
788 early-senescent and non-senescent respectively. **D)** UMAP embedding characterizing the
789 fully senescent, early-senescent, and non-senescent populations in patient cells. **E)** Radar
790 plot of DEGs of senescent (red) versus non-senescent (blue) cells. Expression of the DEGs
791 in the control cells are shown in green. Y-axis represents the log₂ of the expression fold
792 change. Dotted line delineates the threshold of log₂FC = 1.2.



794 **Figure 3: MuSC senescence is a hallmark of DM1 *in vitro* and *in situ*.** **A)** Representative
795 micrographs of primary myoblast culture of one control individual (right image) and one
796 DM1 patient (left image) enzymatically stained for AlexaFluor 488 SA- β -Gal to identify
797 senescent cells (green). Scale bar: 300 μ m. **B)** Quantification of the percentage of SA- β -
798 Gal+ cells ($n = 4-6$); $**p = 0.0023$. **C)** Quantitative real-time PCR for the senescence
799 markers *P16* and *P21* in primary myoblasts from controls and DM1 patients ($n = 3-4$); $*p$
800 = 0.046. **D)** Growth curve of control and DM1 myoblasts cultured *in vitro* for 7 days; $*p$
801 = 0.042. **E)** Representative micrograph of co-immunostaining for RNA FISH (CUG
802 repeats, red), SA- β -Gal (green), and DAPI (blue). Red dashed lines identify a senescent
803 cell and grey dashed lines a non-senescent cell. **F)** Quantification of the number of
804 intranuclear RNA foci per senescent or non-senescent cell in DM1 myoblasts. $**p =$
805 0.0017. **G)** Co-immunofluorescence labeling of PAX7 (green, MuSC marker) and P16
806 (magenta, senescence marker) on muscle sections of a control (upper images) and a DM1
807 patient (bottom images). White arrowheads indicate PAX7+P16- MuSC and white arrows
808 indicate PAX7+P16+ senescent MuSC. Scale bars: 50 μ m. **H)** Quantification of senescent
809 MuSC expressing PAX7 and P16; $*p = 0.0219$. **I)** Quantitative real-time PCR for the
810 senescence markers *P16* ($**p = 0.0075$), and *P21* ($**p = 0.004$) on muscle biopsies from
811 controls and DM1 patients ($n = 5-9$). Data are expressed as means +/- SEM.
812

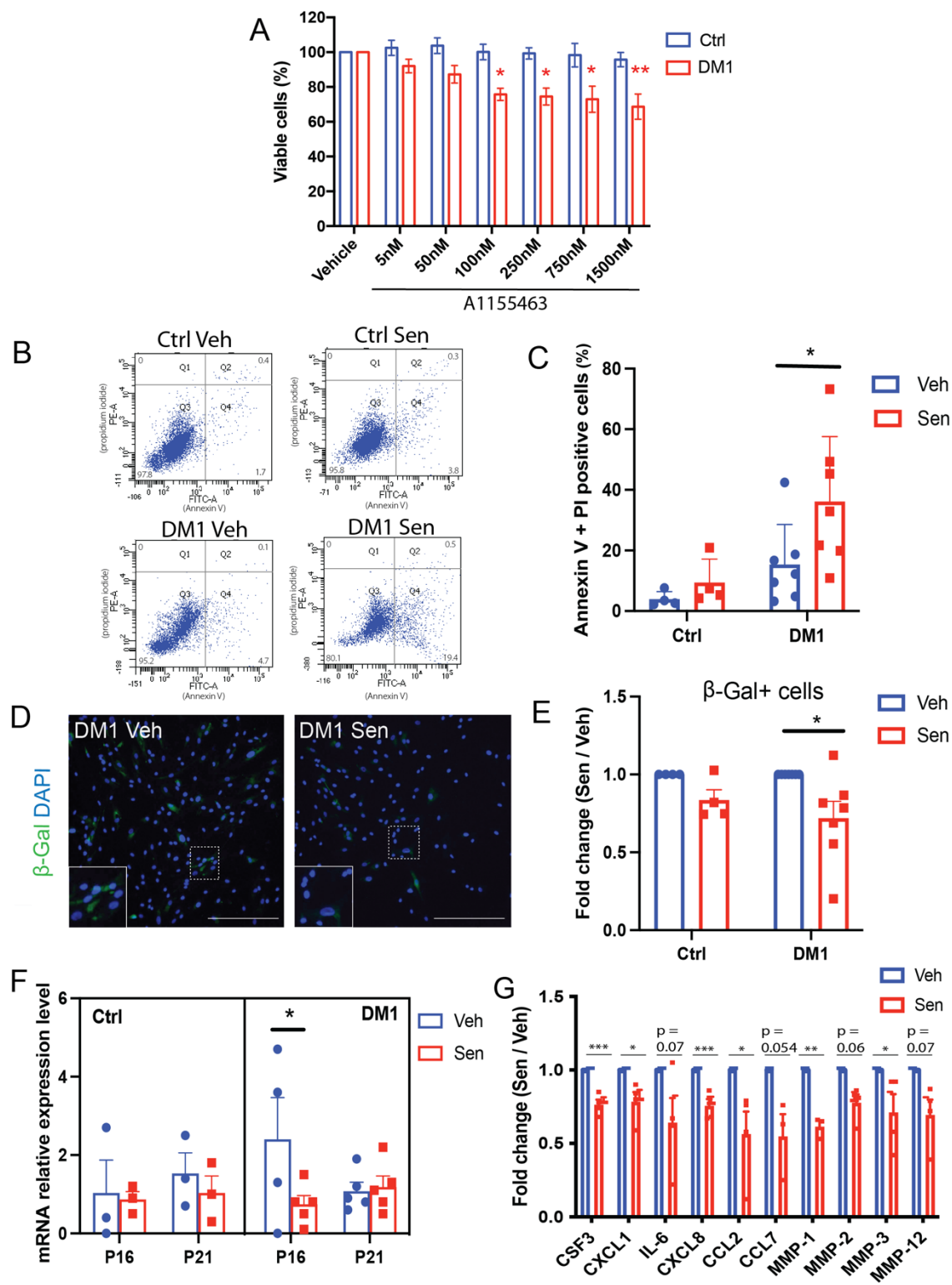
813
814



815
816
817
818
819
820
821

Figure 4. SASP expression is negatively correlated with muscle strength and functional outcomes in DM1. **A-D)** Correlation between serum IL-6 levels in DM1 patients and the expected strength (relative to normative values) of different muscle groups of the lower limb (ankle dorsiflexors, hip flexors, knee extensors, knee flexors) and **E-H)** upper limb (shoulder flexors, shoulder abductors, elbow flexors, elbow extensors). **I)** IL-6 expression levels in the blood serum of DM1 patients. Patients were classified in low- or

822 high-expressing group based on the reference limit for healthy individuals (4.45 pg/ml,
823 indicated by the dashed line). **J,K**) Expected muscle strength of DM1 patients with low or
824 high levels of IL-6 for the lower limb (**J**) and upper limb (**K**) muscle groups. Dashed line
825 indicates the normative data for isometric muscle strength in healthy individuals of the
826 same age, sex, and weight. **L,N,P,R**) Correlation between serum IL-6 levels in DM1
827 patients and the results to different functional capacity tests: Timed-up and Go, 10-meter
828 walk test (10mWT), Berg Balance scale, pinch test. **M,O,Q,S**) Functional capacity test
829 results for DM1 patients with low or high levels of IL-6 levels. **I-K,M,O,Q,S**) Data are
830 expressed as means +/- SEM. N=103 patients (80 patients IL-6 low, 23 patients IL-6 high).
831 *p<0.05, **p<0.01, *** p<0.001.
832
833



834

835

836

837

838

Figure 5: A1155463 shows senolytic activity on DM1 primary myoblasts culture. A) Cell viability assay of A1155463 at different concentrations using control (Ctrl) and DM1 patients' myoblasts. * $p = 0.038$ (100 nM), * $p=0.023$ (250 nM), * $p=0.011$ (750 nM), ** $p=0.0016$ (1500 nM). **B)** Representative FACS plot of Annexin-V (FITC) and

839 propidium iodide (PE), and **C)** quantification of the percentage of positive
840 apoptotic/necrotic cells after 48 h treatment of myoblasts (DM1 and Ctrl) with 100 nM of
841 A1155463 or with vehicle; * $p = 0.034$. **D)** Representative micrographs of DM1 myoblasts
842 stained for the senescent marker SA- β -Gal (green) after 72 h treatment with 100 nM of
843 A1155463 or with vehicle. Scale bar: 300 μ m. **E)** Quantification of the number of SA- β -
844 Gal+ cells expressed as fold change ratio of A1155463-treated (Sen) versus non-treated
845 (Veh) cells (n = 4-7). * $p = 0.015$. **F)** Quantitative real-time PCR for the senescence markers
846 *P16* and *P21* on primary myoblasts after 72 h of treatment with vehicle or A1155463. * p
847 = 0.042. **G)** Multiplex luminex assay of SASP factors showing fold change ratio of
848 A1155463-treated (Sen) versus non-treated (Veh) DM1 myoblasts (n = 3-4). *** $p = 0.0005$
849 (CSF3), * $p = 0.018$ (CXCL1), *** $p = 0.002$ (CXCL8), * $p = 0.041$ (CCL2), ** $p = 0.009$
850 (MMP-1), * $p = 0.027$ (MMP-3). Data are expressed as means +/- SEM.
851
852

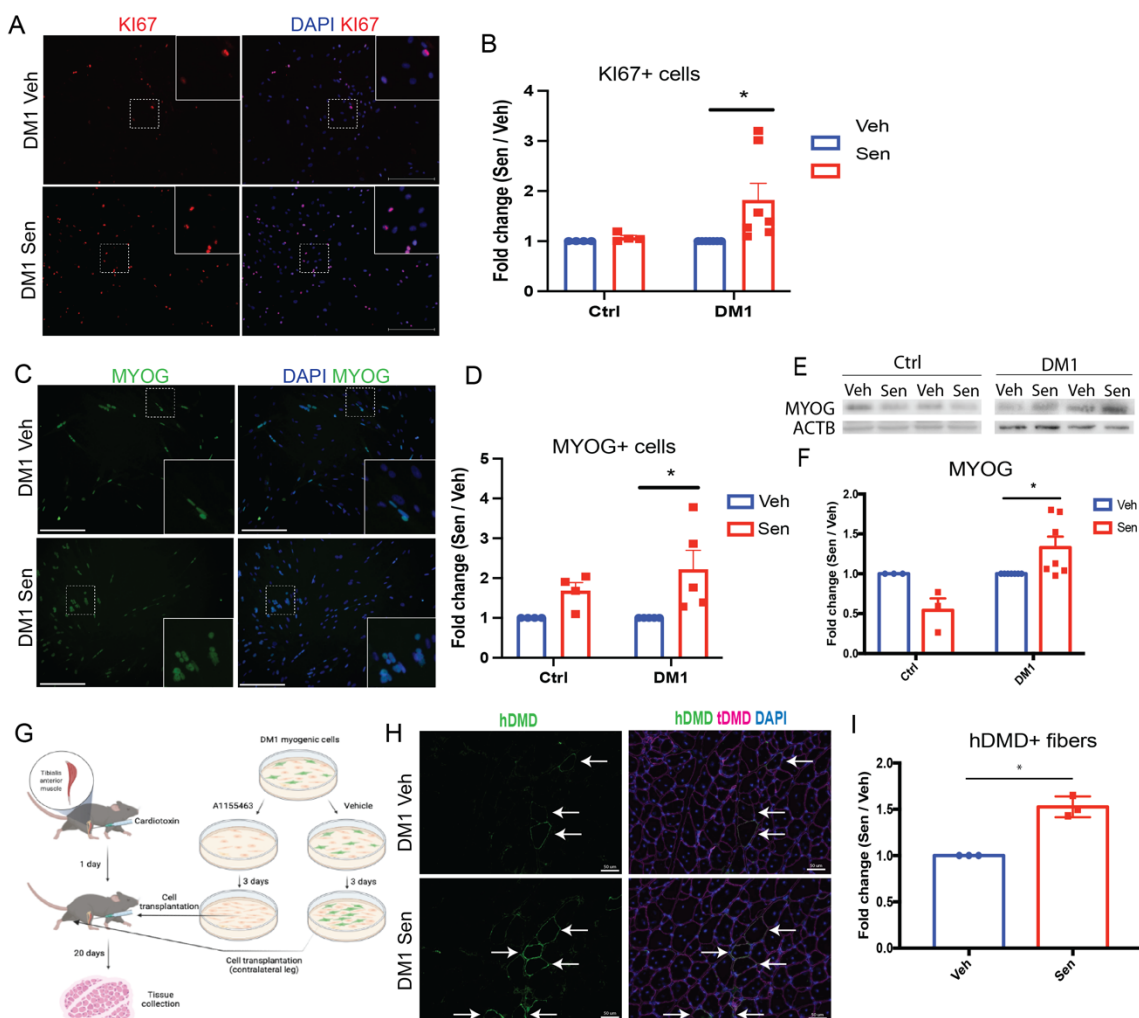


Figure 6: Clearance of senescent cells in DM1 improves myogenesis *in vitro* and *in vivo*. **A)** Representative micrographs of DM1 myoblasts immunolabeled with KI67 (proliferation marker, red) after 72 h of treatment with vehicle (Veh) or A1155463 (Sen). Scale bar: 300 μ m. **B)** Quantification of the proportion of KI67+ cells expressed as fold change ratio of A1155463-treated (Sen) versus non-treated (Veh) cells ($n = 4-7$). * $p = 0.017$. **C)** Representative micrographs of DM1 myoblasts differentiated for 5 days after treatment with vehicle (Veh) or A1155463 (Sen) and immunolabeled with MYOG (differentiation marker, green). Scale bar: 300 μ m. **D)** Quantification of the number of MYOG+ cells expressed as fold change ratio of A1155463-treated (Sen) versus non-treated (Veh) cells ($n = 4-5$). * $p = 0.0134$. **E)** Representative Western blot showing the expression of MYOG in control and DM1 myoblasts differentiated for 5 days after treatment with vehicle (Veh) or A1155463 (Sen). **F)** Quantification of MYOG expression by Western blot (relative to β -actin as loading control). Data are expressed as fold change ratio of A1155463-treated (Sen) versus non-treated (Veh) cells ($n = 3-7$). * $p = 0.039$. **G)** Schematic representation of DM1 myoblast transplantation experiment. **H)** Representative micrographs of muscle sections of TA muscles (21 days post-cardiotoxin injection) of NSG mice transplanted with DM1 myoblasts treated with vehicle (Veh, upper images) or Sen (lower images). hDMD (green), tDMD (magenta), and DAPI (blue) are used for staining. White arrows indicate transplanted tissue. **I)** Bar graph showing fold change of hDMD+ fibers in Sen compared to Veh. Veh shows low fold change (~1.0). Sen shows significantly higher fold change (~1.5) compared to Veh (~1.0).

872 A1155463 (Sen, bottom images). Sections were immunostained with human dystrophin
873 (green), total dystrophin (red), and DAPI (nuclei, blue). White arrows indicate myofibers
874 expressing human and total dystrophin. Scale bar: 50 μ m. **I**) Quantification of the number
875 of myofibers expressing human dystrophin expressed as fold change ratio of A1155463-
876 treated (Sen) versus non-treated (Veh) cells ($n = 3$). * $p = 0.014$. Data are expressed as
877 means +/- SEM

878 **REFERENCES**

- 879 1 Bouchard, G., Roy, R., Declos, M., Mathieu, J. & Kouladjian, K. Origin and
880 diffusion of the myotonic dystrophy gene in the Saguenay region (Quebec). *Can J
881 Neurol Sci* **16**, 119-122, doi:10.1017/s0317167100028651 (1989).
- 882 2 Liao, Q., Zhang, Y., He, J. & Huang, K. Global prevalence of myotonic dystrophy:
883 an updated systematic review and meta-analysis. *Neuroepidemiology* (2022).
- 884 3 Fu, Y. H. *et al.* An unstable triplet repeat in a gene related to myotonic muscular
885 dystrophy. *Science* **255**, 1256-1258, doi:10.1126/science.1546326 (1992).
- 886 4 Savic, D. *et al.* 250 CTG repeats in DMPK is a threshold for correlation of
887 expansion size and age at onset of juvenile-adult DM1. *Hum Mutat* **19**, 131-139,
888 doi:10.1002/humu.10027 (2002).
- 889 5 Thornell, L. E. *et al.* Satellite cell dysfunction contributes to the progressive muscle
890 atrophy in myotonic dystrophy type 1. *Neuropathol Appl Neurobiol* **35**, 603-613,
891 doi:10.1111/j.1365-2990.2009.01014.x (2009).
- 892 6 Hunter, A. *et al.* The correlation of age of onset with CTG trinucleotide repeat
893 amplification in myotonic dystrophy. *J Med Genet* **29**, 774-779,
894 doi:10.1136/jmg.29.11.774 (1992).
- 895 7 Tsilfidis, C., MacKenzie, A. E., Mettler, G., Barcelo, J. & Korneluk, R. G.
896 Correlation between CTG trinucleotide repeat length and frequency of severe
897 congenital myotonic dystrophy. *Nat Genet* **1**, 192-195, doi:10.1038/ng0692-192
898 (1992).
- 899 8 De Antonio, M. *et al.* Unravelling the myotonic dystrophy type 1 clinical spectrum:
900 a systematic registry-based study with implications for disease classification. *Revue
901 neurologique* **172**, 572-580 (2016).
- 902 9 Gagnon, C. *et al.* A 9-year follow-up study of quantitative muscle strength changes
903 in myotonic dystrophy type 1. *J Neurol* **265**, 1698-1705, doi:10.1007/s00415-018-
904 8898-4 (2018).
- 905 10 Dumont, N. A., Bentzinger, C. F., Sincennes, M. C. & Rudnicki, M. A. Satellite
906 Cells and Skeletal Muscle Regeneration. *Compr Physiol* **5**, 1027-1059,
907 doi:10.1002/cphy.c140068 (2015).
- 908 11 Meinke, P., Hintze, S., Limmer, S. & Schoser, B. Myotonic Dystrophy-A Progeroid
909 Disease? *Front Neurol* **9**, 601, doi:10.3389/fneur.2018.00601 (2018).
- 910 12 Bigot, A. *et al.* Large CTG repeats trigger p16-dependent premature senescence in
911 myotonic dystrophy type 1 muscle precursor cells. *Am J Pathol* **174**, 1435-1442,
912 doi:10.2353/ajpath.2009.080560 (2009).
- 913 13 Renna, L. V. *et al.* Premature senescence in primary muscle cultures of myotonic
914 dystrophy type 2 is not associated with p16 induction. *Eur J Histochem* **58**, 2444,
915 doi:10.4081/ejh.2014.2444 (2014).
- 916 14 Hasuike, Y., Mochizuki, H. & Nakamori, M. Expanded CUG Repeat RNA Induces
917 Premature Senescence in Myotonic Dystrophy Model Cells. *Front Genet* **13**,
918 865811, doi:10.3389/fgene.2022.865811 (2022).
- 919 15 Munoz-Espin, D. & Serrano, M. Cellular senescence: from physiology to
920 pathology. *Nat Rev Mol Cell Biol* **15**, 482-496, doi:10.1038/nrm3823 (2014).

- 921 16 Coppé, J.-P. *et al.* Senescence-associated secretory phenotypes reveal cell-
922 nonautonomous functions of oncogenic RAS and the p53 tumor suppressor. *PLoS*
923 *biology* **6**, e301 (2008).
- 924 17 Haddad, F., Zaldivar, F., Cooper, D. M. & Adams, G. R. IL-6-induced skeletal
925 muscle atrophy. *J Appl Physiol (1985)* **98**, 911-917,
926 doi:10.1152/japplphysiol.01026.2004 (2005).
- 927 18 Bian, A. L. *et al.* A study on relationship between elderly sarcopenia and
928 inflammatory factors IL-6 and TNF-alpha. *Eur J Med Res* **22**, 25,
929 doi:10.1186/s40001-017-0266-9 (2017).
- 930 19 Tierney, M. T. *et al.* STAT3 signaling controls satellite cell expansion and skeletal
931 muscle repair. *Nat Med* **20**, 1182-1186, doi:10.1038/nm.3656 (2014).
- 932 20 Baker, D. J. *et al.* Naturally occurring p16(Ink4a)-positive cells shorten healthy
933 lifespan. *Nature* **530**, 184-189, doi:10.1038/nature16932 (2016).
- 934 21 de Keizer, P. L. The Fountain of Youth by Targeting Senescent Cells? *Trends Mol
935 Med* **23**, 6-17, doi:10.1016/j.molmed.2016.11.006 (2017).
- 936 22 Baker, D. J. *et al.* Clearance of p16Ink4a-positive senescent cells delays ageing-
937 associated disorders. *Nature* **479**, 232-236, doi:10.1038/nature10600 (2011).
- 938 23 van Deursen, J. M. Senolytic therapies for healthy longevity. *Science* **364**, 636-637,
939 doi:10.1126/science.aaw1299 (2019).
- 940 24 Xu, M. *et al.* Senolytics improve physical function and increase lifespan in old age.
941 *Nat Med* **24**, 1246-1256, doi:10.1038/s41591-018-0092-9 (2018).
- 942 25 Gallais, B., Gagnon, C., Mathieu, J. & Richer, L. Cognitive decline over time in
943 adults with myotonic dystrophy type 1: a 9-year longitudinal study. *Neuromuscular
944 Disorders* **27**, 61-72 (2017).
- 945 26 Mateos-Aierdi, A. J. *et al.* Muscle wasting in myotonic dystrophies: a model of
946 premature aging. *Front Aging Neurosci* **7**, 125, doi:10.3389/fnagi.2015.00125
947 (2015).
- 948 27 De Buck, M. *et al.* The cytokine-serum amyloid A-chemokine network. *Cytokine
949 Growth Factor Rev* **30**, 55-69, doi:10.1016/j.cytoegr.2015.12.010 (2016).
- 950 28 Binet, F. *et al.* Neutrophil extracellular traps target senescent vasculature for tissue
951 remodeling in retinopathy. *Science* **369**, doi:10.1126/science.aay5356 (2020).
- 952 29 Freund, A., Orjalo, A. V., Desprez, P. Y. & Campisi, J. Inflammatory networks
953 during cellular senescence: causes and consequences. *Trends Mol Med* **16**, 238-
954 246, doi:10.1016/j.molmed.2010.03.003 (2010).
- 955 30 Basisty, N. *et al.* A proteomic atlas of senescence-associated secretomes for aging
956 biomarker development. *PLoS Biol* **18**, e3000599,
957 doi:10.1371/journal.pbio.3000599 (2020).
- 958 31 Hogrel, J. Y. *et al.* Development of a French isometric strength normative database
959 for adults using quantitative muscle testing. *Arch Phys Med Rehabil* **88**, 1289-1297,
960 doi:10.1016/j.apmr.2007.07.011 (2007).
- 961 32 Todd, J., Simpson, P., Estis, J., Torres, V. & Wub, A. H. Reference range and short-
962 and long-term biological variation of interleukin (IL)-6, IL-17A and tissue necrosis
963 factor-alpha using high sensitivity assays. *Cytokine* **64**, 660-665,
964 doi:10.1016/j.cyto.2013.09.018 (2013).
- 965 33 Roussel, M. P., Hebert, L. J. & Duchesne, E. Intra-Rater Reliability and Concurrent
966 Validity of Quantified Muscle Testing for Maximal Knee Extensors Strength in

- 967 968 Men with Myotonic Dystrophy Type 1. *J Neuromuscul Dis* **6**, 233-240,
doi:10.3233/JND-190388 (2019).
- 969 970 34 Knak, K. L., Sheikh, A. M., Andersen, H., Witting, N. & Vissing, J. Intrarater
reliability and validity of outcome measures in myotonic dystrophy type 1.
Neurology **94**, e2508-e2520, doi:10.1212/WNL.0000000000009625 (2020).
- 971 972 35 Zhu, M., Meng, P., Ling, X. & Zhou, L. Advancements in therapeutic drugs
targeting of senescence. *Ther Adv Chronic Dis* **11**, 2040622320964125,
doi:10.1177/2040622320964125 (2020).
- 973 974 36 Baar, M. P. *et al.* Targeted Apoptosis of Senescent Cells Restores Tissue
Homeostasis in Response to Chemotoxicity and Aging. *Cell* **169**, 132-147 e116,
doi:10.1016/j.cell.2017.02.031 (2017).
- 975 976 37 Zhu, Y. *et al.* New agents that target senescent cells: the flavone, fisetin, and the
BCL-XL inhibitors, A1331852 and A1155463. *Aging (Albany NY)* **9**, 955-963,
doi:10.18632/aging.101202 (2017).
- 977 38 Chang, J. *et al.* Clearance of senescent cells by ABT263 rejuvenates aged
hematopoietic stem cells in mice. *Nat Med* **22**, 78-83, doi:10.1038/nm.4010 (2016).
- 978 39 Saito, Y. & Chikenji, T. S. Diverse Roles of Cellular Senescence in Skeletal Muscle
Inflammation, Regeneration, and Therapeutics. *Front Pharmacol* **12**, 739510,
doi:10.3389/fphar.2021.739510 (2021).
- 979 40 Nakamori, M. *et al.* Aberrant Myokine Signaling in Congenital Myotonic
Dystrophy. *Cell Rep* **21**, 1240-1252, doi:10.1016/j.celrep.2017.10.018 (2017).
- 980 41 Usuki, F. & Ishiura, S. Expanded CTG repeats in myotonin protein kinase increase
susceptibility to oxidative stress. *Neuroreport* **9**, 2291-2296,
doi:10.1097/00001756-199807130-00027 (1998).
- 981 42 Toscano, A. *et al.* Oxidative stress in myotonic dystrophy type 1. *Free Radic Res*
39, 771-776, doi:10.1080/10715760500138932 (2005).
- 982 43 Ihara, Y. *et al.* Free radicals, lipid peroxides and antioxidants in blood of patients
with myotonic dystrophy. *J Neurol* **242**, 119-122, doi:10.1007/BF00936882
(1995).
- 983 44 La Rosa, P., Petrillo, S., Bertini, E. S. & Piemonte, F. Oxidative Stress in DNA
Repeat Expansion Disorders: A Focus on NRF2 Signaling Involvement.
Biomolecules **10**, doi:10.3390/biom10050702 (2020).
- 984 45 Roma-Mateo, C. *et al.* Oxidative Stress and the Epigenetics of Cell Senescence:
Insights from Progeroid Syndromes. *Curr Pharm Des* **24**, 4755-4770,
doi:10.2174/1381612824666190114164117 (2018).
- 985 46 Yang, S. R., Park, J. R. & Kang, K. S. Reactive Oxygen Species in Mesenchymal
Stem Cell Aging: Implication to Lung Diseases. *Oxid Med Cell Longev* **2015**,
486263, doi:10.1155/2015/486263 (2015).
- 986 47 Todorow, V. *et al.* Transcriptome Analysis in a Primary Human Muscle Cell
Differentiation Model for Myotonic Dystrophy Type 1. *Int J Mol Sci* **22**,
doi:10.3390/ijms22168607 (2021).
- 987 48 Wang, E. T. *et al.* Transcriptome alterations in myotonic dystrophy skeletal muscle
and heart. *Hum Mol Genet* **28**, 1312-1321, doi:10.1093/hmg/ddy432 (2019).
- 988 49 Espinosa-Espinosa, J., Gonzalez-Barriga, A., Lopez-Castel, A. & Artero, R.
Deciphering the Complex Molecular Pathogenesis of Myotonic Dystrophy Type 1
through Omics Studies. *Int J Mol Sci* **23**, doi:10.3390/ijms23031441 (2022).

- 1013 50 Franck, S. *et al.* Myotonic dystrophy type 1 embryonic stem cells show decreased
1014 myogenic potential, increased CpG methylation at the DMPK locus and RNA mis-
1015 splicing. *Biol Open* **11**, doi:10.1242/bio.058978 (2022).
- 1016 51 Andre, L. M. *et al.* Recovery in the Myogenic Program of Congenital Myotonic
1017 Dystrophy Myoblasts after Excision of the Expanded (CTG)n Repeat. *Int J Mol Sci*
1018 **20**, doi:10.3390/ijms20225685 (2019).
- 1019 52 Rivera-Mulia, J. C. *et al.* DNA replication timing alterations identify common
1020 markers between distinct progeroid diseases. *Proc Natl Acad Sci U S A* **114**,
1021 E10972-E10980, doi:10.1073/pnas.1711613114 (2017).
- 1022 53 Otero, B. A. *et al.* Transcriptome alterations in myotonic dystrophy frontal cortex.
1023 *Cell Rep* **34**, 108634, doi:10.1016/j.celrep.2020.108634 (2021).
- 1024 54 Hari, P. *et al.* The innate immune sensor Toll-like receptor 2 controls the
1025 senescence-associated secretory phenotype. *Science advances* **5**, eaaw0254 (2019).
- 1026 55 Kirkland, J. L. & Tchkonia, T. Senolytic drugs: from discovery to translation. *J
1027 Intern Med* **288**, 518-536, doi:10.1111/joim.13141 (2020).
- 1028 56 Ge, M. *et al.* Senolytic targets and new strategies for clearing senescent cells. *Mech
1029 Ageing Dev* **195**, 111468, doi:10.1016/j.mad.2021.111468 (2021).
- 1030 57 Sevilla, L., Zaldumbide, A., Pognonec, P. & Boulukos, K. Transcriptional
1031 regulation of the bcl-x gene encoding the anti-apoptotic Bcl-xL protein by Ets,
1032 Rel/NFKB STAT and AP1 transcription factor families. *Histology and
1033 histopathology* (2001).
- 1034 58 Gros, M. *et al.* Identification of Serum Interleukin 6 Levels as a Disease Severity
1035 Biomarker in Facioscapulohumeral Muscular Dystrophy. *J Neuromuscul Dis* **9**, 83-
1036 93, doi:10.3233/JND-210711 (2022).
- 1037 59 Overend, G. *et al.* Allele length of the DMPK CTG repeat is a predictor of
1038 progressive myotonic dystrophy type 1 phenotypes. *Hum Mol Genet* **28**, 2245-
1039 2254, doi:10.1093/hmg/ddz055 (2019).
- 1040 60 Sugihara, H., Teramoto, N., Yamanouchi, K., Matsuwaki, T. & Nishihara, M.
1041 Oxidative stress-mediated senescence in mesenchymal progenitor cells causes the
1042 loss of their fibro/adipogenic potential and abrogates myoblast fusion. *Aging
1043 (Albany NY)* **10**, 747-763, doi:10.18632/aging.101425 (2018).
- 1044 61 Pascual-Gilabert, M., López-Castel, A. & Artero, R. Myotonic dystrophy type 1
1045 drug development: A pipeline toward the market. *Drug Discovery Today* **26**, 1765-
1046 1772 (2021).
- 1047 62 Petitclerc, E., Hebert, L. J., Mathieu, J., Desrosiers, J. & Gagnon, C. Lower limb
1048 muscle strength impairment in late-onset and adult myotonic dystrophy type 1
1049 phenotypes. *Muscle Nerve* **56**, 57-63, doi:10.1002/mus.25451 (2017).
- 1050 63 Jimenez-Moreno, A. C. *et al.* Analysis of the functional capacity outcome measures
1051 for myotonic dystrophy. *Ann Clin Transl Neurol* **6**, 1487-1497,
1052 doi:10.1002/acn3.50845 (2019).
- 1053 64 Raymond, K. *et al.* Predictors of participation restriction over a 9-year period in
1054 adults with myotonic dystrophy type 1. *Disabil Rehabil*, 1-17,
1055 doi:10.1080/09638288.2020.1837264 (2020).
- 1056 65 Shanely, R. A. *et al.* Human skeletal muscle biopsy procedures using the modified
1057 Bergstrom technique. *J Vis Exp*, 51812, doi:10.3791/51812 (2014).

- 1058 66 Sasarman, F., Karpati, G. & Shoubridge, E. A. Nuclear genetic control of
1059 mitochondrial translation in skeletal muscle revealed in patients with mitochondrial
1060 myopathy. *Hum Mol Genet* **11**, 1669-1681, doi:10.1093/hmg/11.14.1669 (2002).
1061 67 Alexander, M. S. *et al.* CD82 Is a Marker for Prospective Isolation of Human
1062 Muscle Satellite Cells and Is Linked to Muscular Dystrophies. *Cell Stem Cell* **19**,
1063 800-807, doi:10.1016/j.stem.2016.08.006 (2016).
1064 68 Zarkada, G. *et al.* Specialized endothelial tip cells guide neuroretina vascularization
1065 and blood-retina-barrier formation. *Dev Cell* **56**, 2237-2251 e2236,
1066 doi:10.1016/j.devcel.2021.06.021 (2021).
1067 69 Zheng, G. X. *et al.* Massively parallel digital transcriptional profiling of single cells.
1068 *Nat Commun* **8**, 14049, doi:10.1038/ncomms14049 (2017).
1069 70 Hao, Y. *et al.* Integrated analysis of multimodal single-cell data. *Cell* **184**, 3573-
1070 3587 e3529, doi:10.1016/j.cell.2021.04.048 (2021).
1071 71 Brennecke, P. *et al.* Accounting for technical noise in single-cell RNA-seq
1072 experiments. *Nat Methods* **10**, 1093-1095, doi:10.1038/nmeth.2645 (2013).
1073 72 McGinnis, C. S., Murrow, L. M. & Gartner, Z. J. DoubletFinder: Doublet Detection
1074 in Single-Cell RNA Sequencing Data Using Artificial Nearest Neighbors. *Cell Syst*
1075 **8**, 329-337 e324, doi:10.1016/j.cels.2019.03.003 (2019).
1076 73 Blondel, V. D., Guillaume, J.-L., Lambiotte, R. & Lefebvre, E. Fast unfolding of
1077 communities in large networks. *Journal of Statistical Mechanics: Theory and
1078 Experiment* **2008**, P10008, doi:10.1088/1742-5468/2008/10/p10008 (2008).
1079 74 van der Maaten, L. & Hinton, G. Visualizing data using t-SNE. *Journal of Machine
1080 Learning Research* **9**, 2579-2605 (2008).
1081 75 Benjamini, Y. & Hochberg, Y. Controlling the False Discovery Rate: A Practical
1082 and Powerful Approach to Multiple Testing. *Journal of the Royal Statistical
1083 Society: Series B (Methodological)* **57**, 289-300,
1084 doi:<https://doi.org/10.1111/j.2517-6161.1995.tb02031.x> (1995).
1085 76 Finak, G. *et al.* MAST: a flexible statistical framework for assessing transcriptional
1086 changes and characterizing heterogeneity in single-cell RNA sequencing data.
1087 *Genome Biol* **16**, 278, doi:10.1186/s13059-015-0844-5 (2015).
1088 77 Zhou, Y. *et al.* Metascape provides a biologist-oriented resource for the analysis of
1089 systems-level datasets. *Nat Commun* **10**, 1523, doi:10.1038/s41467-019-09234-6
1090 (2019).
1091 78 Yu, G. & He, Q. Y. ReactomePA: an R/Bioconductor package for reactome
1092 pathway analysis and visualization. *Mol Biosyst* **12**, 477-479,
1093 doi:10.1039/c5mb00663e (2016).
1094 79 Hanzelmann, S., Castelo, R. & Guinney, J. GSVA: gene set variation analysis for
1095 microarray and RNA-seq data. *BMC Bioinformatics* **14**, 7, doi:10.1186/1471-2105-
1096 14-7 (2013).
1097 80 Ashburner, M. *et al.* Gene ontology: tool for the unification of biology. The Gene
1098 Ontology Consortium. *Nat Genet* **25**, 25-29, doi:10.1038/75556 (2000).
1099 81 Gene Ontology, C. The Gene Ontology resource: enriching a GOld mine. *Nucleic
1100 Acids Res* **49**, D325-D334, doi:10.1093/nar/gkaa1113 (2021).
1101 82 Fridman, A. L. & Tainsky, M. A. Critical pathways in cellular senescence and
1102 immortalization revealed by gene expression profiling. *Oncogene* **27**, 5975-5987,
1103 doi:10.1038/onc.2008.213 (2008).

- 1104 83 Xia, G. *et al.* Generation of neural cells from DM1 induced pluripotent stem cells
1105 as cellular model for the study of central nervous system neuropathogenesis.
1106 *Cellular reprogramming* **15**, 166-177 (2013).
- 1107 84 Bhatnagar, S., Panguluri, S. K. & Kumar, A. Gene profiling studies in skeletal
1108 muscle by quantitative real-time polymerase chain reaction assay. *Methods Mol
1109 Biol* **798**, 311-324, doi:10.1007/978-1-61779-343-1_18 (2012).
- 1110 85 Stern-Straeter, J., Bonaterra, G. A., Hörmann, K., Kinscherf, R. & Goessler, U. R.
1111 Identification of valid reference genes during the differentiation of human
1112 myoblasts. *BMC molecular biology* **10**, 1-9 (2009).
- 1113